



Technisch-Naturwissenschaftliche
Fakultät

Enzyme Immobilization on Electrodes for CO₂ Reduction

Bachelor Thesis

to confer the academic degree of

Bachelor of Science (BSc)

in the bachelor program

Technical Chemistry

Author:

Annika Wagner

Submission:

Institute for Organic Solar Cells / Institute of Physical Chemistry

Thesis supervisor:

o.Univ. Prof. Mag. Dr. DDr. h.c. Niyazi Serdar Sariciftci

Assistant Thesis Supervisor:

DI Stefanie Schager

December 2013

Statement of Authorship

I hereby confirm that this bachelor thesis was written autonomously by me and without foreign help. No other than the cited references were used.

Linz, December 2013

Abstract

Utilization of CO₂ as a chemical feedstock offers a way to reduce greenhouse gases and additionally to produce higher energy molecules, especially methanol and other fuels, and therefore to move towards an independence of fossil fuels. The exploitation of dehydrogenase-enzymes as biocatalysts for CO₂ reduction enables an attractive way to produce formate, formaldehyde and methanol from CO₂. To accomplish stability and reusability, enzymes were immobilized in different matrices. Furthermore, the ambition to replace the expensive cofactor nicotinamide adenine dinucleotide (NADH) as electron donor lead to the idea to immobilize the enzymes on electrode surfaces to directly provide the required electrons from the electrode. A carbonfelt (CF) electrode coated with an alginate-silica hybrid gel containing three different dehydrogenases (formate dehydrogenase, F_{ate}DH; formaldehyde dehydrogenase, F_{ald}DH; alcohol dehydrogenase, ADH) was fabricated and methanol was produced during electrolysis in 0.05 M Trizma[®] buffer solution as electrolyte (pH adjusted to 7.64 with HCl) with a faradaic efficiency of about 90%. Further electrolysis experiments were conducted only for the first reaction step from CO₂ to formate, catalyzed by F_{ate}DH for simplicity and cost reasons. A Pt-polypyrrole electrode coated with a F_{ate}DH modified alginate gel and a Pt-polypyrrole electrode with entrapped F_{ate}DH were fabricated. For both electrodes modified with F_{ate}DH, formate production could be achieved with faradaic efficiencies of about 40% and 85% respectively. Moreover, a graphite electrode with adsorbed F_{ate}DH was fabricated, which was however, not capable of producing formate.

Kurzfassung

Die Nutzung von CO₂ als chemischen Rohstoff eröffnet die Möglichkeit, Treibhausgase in der Atmosphäre zu reduzieren und darüber hinaus energiereiche Moleküle zu produzieren, die beispielsweise als Brennstoffe genutzt werden können. Dadurch könnte eine Unabhängigkeit von fossilen Brennstoffen erreicht werden. Dehydrogenasen können verwendet werden, um CO₂ zu Formiat, Formaldehyd und Methanol zu reduzieren. Um Stabilität und Wiederverwendbarkeit der Enzyme zu erreichen, wurden verschiedene Methoden der Immobilisierung in unterschiedlichen Matrices untersucht. Zusätzlich hat das Bestreben den teuren Cofaktor Nicotinamid Adenin Dinucleotid (NADH) als Elektronendonator zu ersetzen zu der Idee geführt, die Enzyme auf einer Elektrodenoberfläche zu immobilisieren, um die benötigten Elektronen direkt von der Elektrode zur Verfügung zu stellen. Eine Kohlenstoff-Filz Elektrode wurde mit einem Alginat-Silikat Hybridgel mit drei verschiedenen Dehydrogenasen (Formiat Dehydrogenase, F_{ate}DH; Formaldehyd Dehydrogenase, F_{ald}DH; Alkoholdehydrogenase, ADH) überzogenen. Während der Elektrolyse mit dieser Elektrode in 0.05 M Trizma[®] Pufferlösung (pH eingestellt auf 7.64 mit HCl) als Elektrolyt wurde Methanol mit einer Faradayeffizienz von ca. 90% produziert. Weitere Elektrolyseexperimente wurden aus Kostengründen nur für den ersten Schritt, also die Reduktion von CO₂ zu Formiat durchgeführt. Mit F_{ate}DH enthaltendem Alginat-Silikat Hybridgel beschichtete Pt-Polypyrrol Elektroden und Pt-Polypyrrol Elektroden mit eingekapselter F_{ate}DH wurden hergestellt und mit beiden Elektroden wurde Formiat mit einer Faradayeffizienzen von ca. 40% bzw 85% produziert. Des Weiteren wurden Graphitelektroden mit adsorbierter F_{ate}DH hergestellt, welche jedoch kein Formiat produzierten.

Table of contents

1. Introduction	1
1.1. Background.....	1
1.1.1. Severity of rising Atmospheric CO ₂	1
1.2. Possibilities of addressing the CO ₂ problem	3
1.2.1. <i>Carbon Capture and Storage</i>	3
1.2.1.1. <i>Carbon Capture</i>	3
1.2.1.2. <i>Carbon Storage</i>	4
1.2.2. <i>Carbon Capture and Utilization</i>	5
1.2.2.1. <i>Electrochemical conversion</i>	6
1.2.2.2. <i>Photochemical conversion</i>	8
1.2.2.3. <i>Biological conversion: Usage of bacteria and enzymes for CO₂ reduction</i>	8
2. Materials and Methods.....	16
2.1. Chemicals.....	17
2.2. Apparatus	17
2.3. CF/Alginate/F _{ate} DH/F _{ald} DH/ADH – Electrodes	18
2.3.1. <i>Fabrication of CF/Alginate/F_{ate}DH/F_{ald}DH/ADH-Electrodes</i>	18
2.3.2. <i>Characterization of CF/Alginate/F_{ate}DH/F_{ald}DH/ADH-Electrodes</i>	19
2.3.3. <i>Electrolysis with CF/Alginate/F_{ate}DH/F_{ald}DH/ADH-Electrodes</i>	19
2.4. Pt/PPy/Alginate/F _{ate} DH – Electrodes	19
2.4.1. <i>Fabrication of Pt/PPy/Alginate/F_{ate}DH-Electrodes</i>	19
2.4.2. <i>Characterization of Pt/PPy/Alginate/F_{ate}DH Electrodes</i>	20
2.4.3. <i>Electrolysis with Pt/PPy/Alginate/F_{ate}DH Electrodes</i>	20
2.5. Pt/PPy/F _{ate} DH – Electrodes	21
2.5.1. <i>Fabrication of Pt/PPy/F_{ate}DH - Electrodes</i>	21
2.5.2. <i>Characterization of Pt/PPy/F_{ate}DH - Electrodes</i>	21
2.5.3. <i>Electrolysis with Pt/PPy/F_{ate}DH - Electrodes</i>	22
2.6. Physical Adsorption of F _{ate} DH on Graphite Rods.....	22
2.6.1. <i>Production of Graphite/F_{ate}DH Electrodes</i>	22
2.6.2. <i>Characterization of Graphite/F_{ate}DH Electrodes</i>	22
2.6.3. <i>Electrolysis with Graphite/F_{ate}DH Electrodes</i>	23
3. Results and Discussion.....	23
3.1. CF/Alginate/F _{ate} DH/F _{ald} DH/ADH – Electrodes	23
3.1.1. <i>Characterization of CF/Alginate/F_{ate}DH/F_{ald}DH/ADH electrodes</i>	23

3.1.2.	<i>Electrolysis with CF/Alginate/F_{ate}DH/F_{ald}DH/ADH electrodes</i>	27
3.1.3.	<i>Faradaic efficiency of Methanol production at CF/Alginate/F_{ate}DH/F_{ald}DH/ADH electrodes</i>	31
3.1.4.	<i>Stability of CF/Alginate/F_{ate}DH/F_{ald}DH/ADH electrodes</i>	32
3.2.	<i>Pt/PPy/Alginate/F_{ate}DH Electrodes</i>	33
3.2.1.	<i>Characterization of Pt/PPy/F_{ate}DH electrodes</i>	33
3.2.2.	<i>Electrolysis with Pt/PPy/Alginate/F_{ate}DH electrodes</i>	37
3.2.3.	<i>Faradaic efficiency of formate production at Pt/PPy/Alginate/F_{ate}DH electrodes</i>	39
3.2.4.	<i>Stability of Pt/PPy/Alginate/F_{ate}DH electrodes</i>	40
3.3.	<i>Pt/PPy/F_{ate}DH Electrodes</i>	40
3.3.1.	<i>Characterization of Pt/PPy/F_{ate}DH electrodes</i>	40
3.3.2.	<i>Electrolysis with Pt/PPy/F_{ate}DH electrodes</i>	44
3.3.3.	<i>Faradaic efficiency of formate production at Pt/PPy/F_{ate}DH electrodes</i>	47
3.3.4.	<i>Stability of Pt/PPy/F_{ate}DH electrodes</i>	48
3.3.5.	<i>Microscopic characterization of the Pt/PPy/F_{ate}DH electrodes</i>	48
3.4.	<i>Physical Adsorption of F_{ate}DH on Graphite Rods</i>	49
3.4.1.	<i>Characterization of Graphite/F_{ate}DH electrodes</i>	49
3.4.2.	<i>Electrolysis with a Graphite/F_{ate}DH electrode</i>	52
4.	<i>Conclusion</i>	55
5.	<i>Acknowledgements</i>	56
6.	<i>References</i>	56

1. Introduction

1.1. Background

1.1.1. Severity of rising Atmospheric CO₂

Rising CO₂ values in the atmosphere and the resulting global warming in the past decades have made it necessary to develop methods to stop the increase of or even decrease CO₂ levels. Figure 1 shows the trend of atmospheric CO₂ from 1959 to 2013 measured at Mauna Loa Observatory, Hawaii [1].

These measurements were started by C.D. Keeling in 1958 [2].

The red curve displays the carbon dioxide values measured as the mole fraction in dry air in parts per million (ppm). It can be seen that there has been a dramatic rise in atmospheric CO₂ of about 80 ppm in the past 50 years.

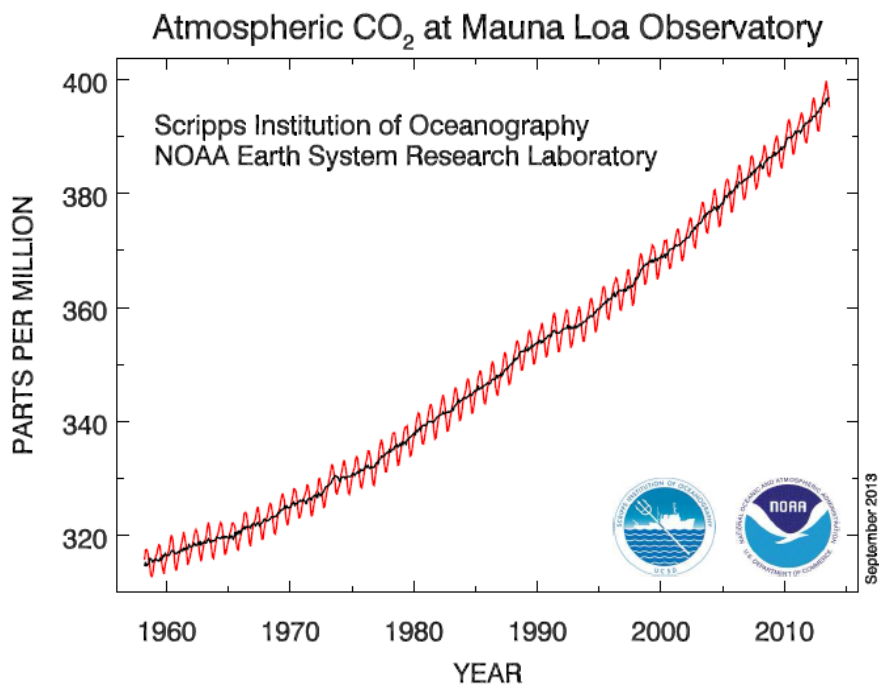


Figure 1: Atmospheric CO₂ levels measured at Mauna Loa Observatory, Hawaii [1].

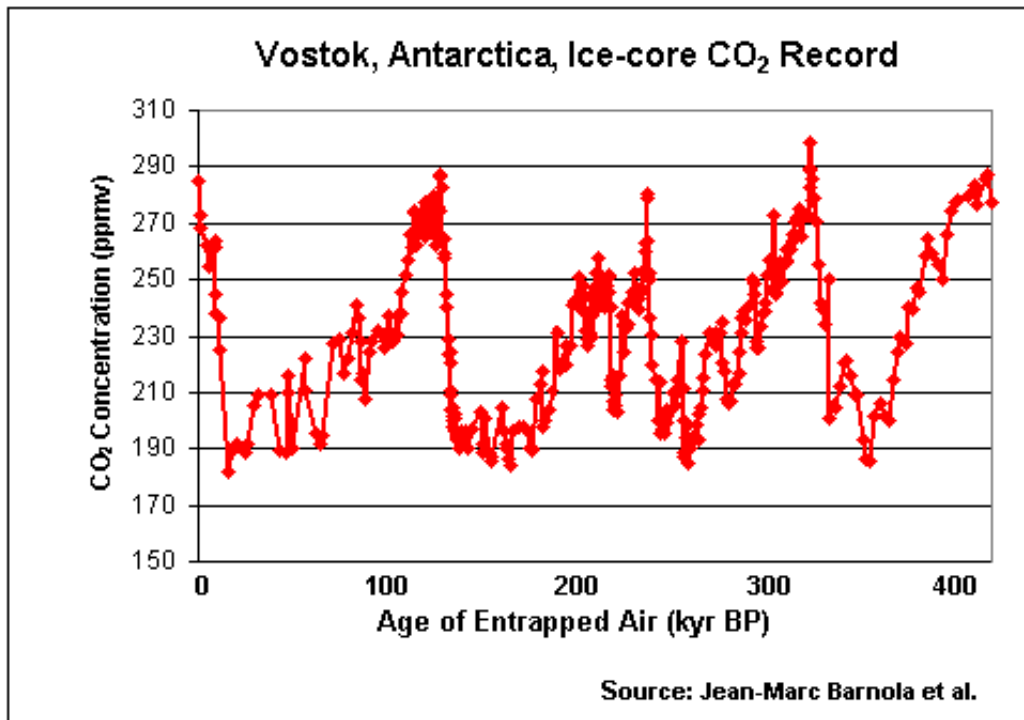


Figure 2: Atmospheric CO₂ concentration of the past 400000 years recorded from measurements of the Vostok ice cores, Antarctica [4].

A method to trace atmospheric CO₂ back to several thousand years is offered by analyzing ice-cores as there are entrapped air inclusions in the ice which enable direct records of past changes in the atmospheric gas composition. Such measurements were performed at the Russian Vostok station in east Antarctica in 1998, where an ice core with a depth of 3623 m was recovered [3, 4].

In Figure 2 the CO₂ concentration in the atmosphere is depicted as a function of kyr BP (1000 years before present). This graph shows again that the levels of CO₂ in the atmosphere have never been as high as they are at present. The highest values in Figure 2 are about 100 ppm lower than the present CO₂ values.

Those records and observations show the close correlation of temperature and atmospheric CO₂ levels as reported by Barnola et al. [5]. This reveals that global warming proceeds with increasing CO₂ levels in the atmosphere and should alert humanity to focus on reducing the CO₂ emissions and thus achieve decreasing CO₂ values in the atmosphere.

1.2. Possibilities of addressing the CO₂ problem

There are several approaches to reduce atmospheric CO₂, which can be divided in mainly two methods. In the Carbon Capture and Storage approach, CO₂ is captured and afterwards stored for example in geological formations or in the ocean. In the Carbon Capture and Sequestration approach, the captured CO₂ is recycled to higher energy molecules.

1.2.1. Carbon Capture and Storage

In the field of Carbon Capture and Storage (CCS) many technologies are currently in research and development. A few technologies have already reached the stage of economic viability but still, most technologies have to be improved concerning technical capabilities and costs [6].

1.2.1.1. Carbon Capture

There are three main approaches for Carbon Capture (see Figure 3): In the process modification method a nearly pure CO₂ stream from either an existing industrial process is captured or a process is reengineered to generate a stream like this. Alternatively, concentration of the discharge from an industrial process into a pure CO₂ stream can be done. The third approach is direct air capture into a pure CO₂ stream or alternatively into a chemically stable end product [6].

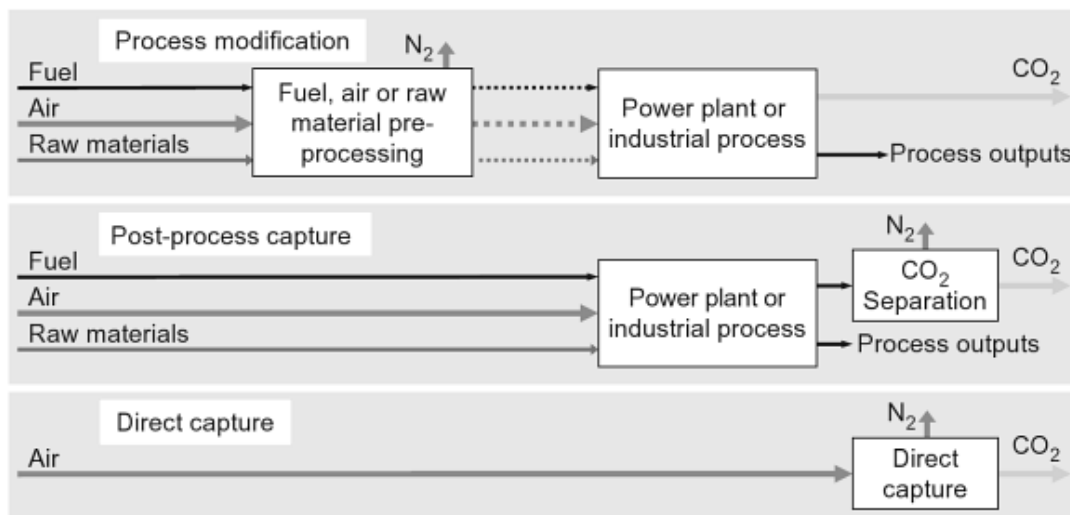


Figure 3 : Three possible methods for CO₂ capture: process modification (CO₂ capture within the industrial process), post process capture (CO₂ separation from process outputs and subsequent capture), direct capture (CO₂ capture directly from air) [6].

1.2.1.2. Carbon Storage

There are several possibilities to store carbon dioxide. In the geological storage approach, which is currently the most used technique for CO₂ storage, direct injection of Carbon Dioxide into oil-, gas- and water-bearing geological formations is performed. This method is also utilized on a commercial scale. Another possibility to store CO₂ is ocean storage, which is, however, more difficult to realize. At the water-surface CO₂ is exchanged with the atmosphere within a time scale of months to years. Therefore the storage has to be done at great depth to ensure that CO₂ is not released back to the atmosphere. A possibility to achieve long-term storage by direct dissolution is to vent gaseous CO₂ or supercritical fluid at the necessary depth to guarantee dispersal of the rising plume before it reaches the surface. This model can be realized either from a fixed pipeline or from a riser appended to a moving ship (See Figure 4).

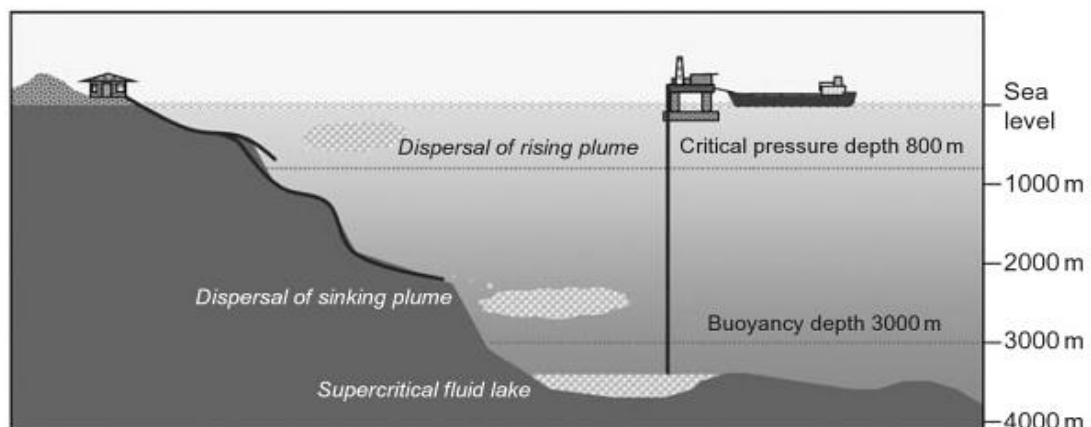


Figure 4: Ocean Storage. In this CO₂ storage approach, CO₂ has to be pumped into great depth in the ocean by a fixed pipeline or a ship to make sure that the CO₂ will not be released back to the atmosphere [6].

An alternative to the mentioned ocean storage method would be storage of CO₂ as a lake of supercritical fluid. This is only feasible if CO₂ is injected below the depth at which it becomes negatively buoyant in seawater, which is in a depth of about 3000 m [6]. Another method to store CO₂ is the storage in terrestrial ecosystems. The idea of CO₂ storage in terrestrial ecosystems is to enhance natural processes that remove CO₂ from the atmosphere, which may be one of the most cost effective means of reducing atmospheric CO₂. Ecosystems which possess a significant potential for carbon sequestration comprise forest lands, agricultural lands, deserts and degraded lands. Carbon can be sequestered by increasing the amount of aboveground biomass in an ecosystem that is for

example converting grasslands to forests, as forests contain a big amount of living biomass. Alternatively, the amount of carbon existing in soils can be enlarged [7].

1.2.2. Carbon Capture and Utilization

Carbon Capture and Utilization is concerned with recycling and conversion of CO₂ to fuels or other valuable organic molecules. Different energies are used to break the C-O bond in carbon dioxide and convert it into useful products, e.g. electricity in the electrochemical reduction and light in the photochemical reduction. There are several possible options which will be discussed briefly in the following.

G. Olah discusses chemical recycling of CO₂ to methanol in his book. Methanol can be obtained by the reduction of CO₂ with H₂ gas. The required CO₂ can be isolated from coal- or fossil fuel burning industrial plants or directly from the atmosphere. However, more efficient methods have to be developed to utilize CO₂ directly from the atmosphere. H₂ can be produced by water electrolysis of sea water. This method would offer a possibility to reach complete independence of fossil fuel sources. Furthermore, production of methanol out of CO₂ and H₂ provides a way to convert the volatile hydrogen gas to a convenient and safe liquid. Further researches mentioned by G. Olah, focus on electrochemical and photocatalytic CO₂ reduction [8].

In another approach M. Aresta presents possible ways to utilize CO₂ as a building block for higher energy molecules. Potential reaction routes are depicted in Figure 5. By the routes A and B, carboxylates, carbamates, and carbonates are obtained by incorporation of the whole CO₂ molecule. These reactions have low energy content and occur at room temperature or lower. By the routes C and D, CO₂ is reduced to other C₁ or C_n molecules. In comparison to A and B these reactions require an input of energy [9].

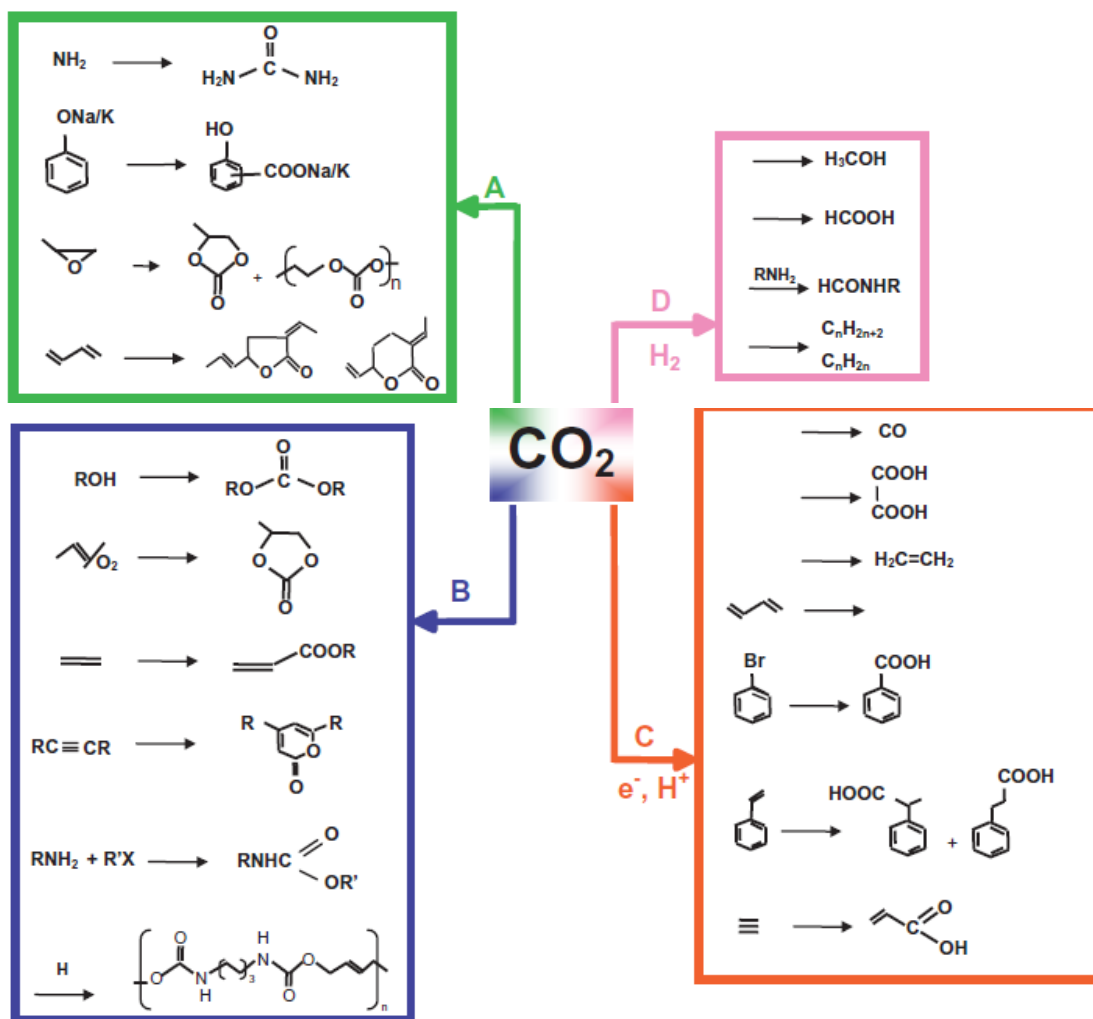
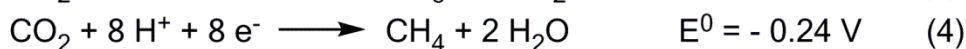
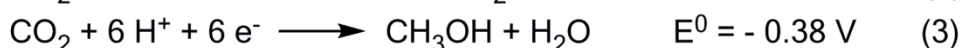
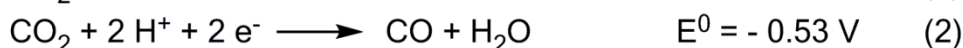


Figure 5: Possible routes for CO₂ conversion: By the routes A and B, carboxylates, carbamates and carbonates are obtained. By the routes C and D, CO₂ is converted to other C1 and C_n molecules. However, in comparison to routes A and B, these reactions require energy and do not occur at room temperature [9].

1.2.2.1. Electrochemical conversion

The reduction of CO₂ is performed via one and multi-electron processes. In electrochemical reduction of carbon dioxide, electrons are provided by electrical energy. Equation 1 depicts the standard redox potentials of the reduction of CO₂ to different products.



Equation 1: CO₂ reduction reactions and their standard potentials at pH 7 in aqueous solution, versus NHE at 25°C and 1 atm [10].

The electrochemical reduction of CO₂ is of special interest, as a carbon neutral energy cycle can be realized. In this way, CO₂ is converted by input of energy to fuels, which can be burned and energy and CO₂ are released again.

The reduction of CO₂, however, requires much higher potentials than the theoretical values in Equation 1. Therefore, to overcome such high overpotentials and to improve current efficiency and selectivity, catalysts are utilized. Catalysis in electrochemical processes can be performed homogeneously or heterogeneously. Homogeneous catalysts are in the same phase as the reaction phase, heterogeneous catalysts are catalyzing reactions in a different phase. A clear advantage of heterogeneous catalysis is that the catalyst can be removed from the reaction system after usage and can be readily reused [10].

Over the last decades a large number of catalysts for electrochemical CO₂ reduction have been developed. Especially in the field of transition metal complexes investigations have been done intensively. The electrocatalytic effect of Rhenium catalysts for CO₂ reduction was first reported by Lehn et al. in 1984 [11]. A great number of transition metal based catalysts were developed, as reported by Benson et al. and Portenkirchner et al., who present a review of rhenium and rhodium complexes for electro- and photocatalytic CO₂ reduction [12, 13].

In transition metal complexes, the catalyst center comprises transition metals based on rhenium, rhodium or ruthenium bound to bipyridine ligands. These molecules enable stabilization of intermediate states of the CO₂ reduction reaction thereby lowering the required overpotential. Another method for electrochemical CO₂ reduction is presented by Cosnier et al. who used rhenium catalysts bound to a polypyrrole film on an electrode [14]. The group of Barton-Cole et al. show the utilization of pyridine alone as catalyst for CO₂ reduction with faradaic efficiencies of 22% [15].

Further approaches for electrochemical CO₂ reduction have been reported by the groups of Mizuno et al. [16] who used ultra high temperatures and methanol as solvent.

1.2.2.2. Photochemical conversion

Photochemical CO₂ reduction uses light as the energy input for the conversion of CO₂ to higher energy products. Methods inspired by this principle are also referred to as artificial photosynthesis-methods. In photosynthesis, CO₂ and light is converted via a complex chain of reactions to glucose, starch, oxygen and water. Recent advances in the field of photochemical CO₂ reduction have been made by Nocera, who has developed a catalyst system to design an artificial leaf which duplicates the process of photosynthesis [17]. The group of Gholamkhash et al. report the usage of ruthenium- rhenium- bi- and tetranuclear complexes for photocatalytic CO₂ reduction [18]. Mao et al. present a review of photocatalytic CO₂ reduction over semiconductors [19].

Furthermore, there have also been researches in the field of photoelectrochemical reduction of CO₂, in which the principles of photochemistry and electrochemistry are combined. T. Arai et al. report the photoelectrochemical reduction of CO₂ to formate by a p-type InP photocathode modified with an electropolymerised ruthenium complex [20]. A similar approach is presented by E. E. Barton et al., who use a p-type GaP semiconductor electrode with a homogeneous pyridinium ion catalyst for selective reduction of CO₂ to methanol [21].

1.2.2.3. Biological conversion: Usage of bacteria and enzymes for CO₂ reduction

In recent works, investigations were made concerning the use of biological catalysts for CO₂ reduction. This approach opens the way to sustainable and biodegradable methods of CO₂ reduction. Several species of bacteria can be used to turn CO₂ into useful chemicals. Ethan I. Lan and James C. Liao [22] present a way to produce isobutanol, a chemical feedstock and potential fuel, from cyanobacteria, utilizing CO₂ and light. Another example for bacterial CO₂ reduction is described by G. Diekert [23]. In this case, homoacetogenic bacteria were used to convert two molecules of CO₂ to acetate. There have also been

investigations on combining bacterial and electrochemical CO₂ reduction. In this field M. Kuroda and T. Watanabe [24] report a CO₂ reduction to methane or acetate by immobilized Methanogens and Homoacetogens on electrodes.

Moreover, enzymes also can be used for CO₂ conversion to useful chemicals. In this field, intensive research has been done by M. Aresta, who contributed to the understanding of the function of carbon monoxide dehydrogenase, which converts CO₂ to CO [25]. He also discovered that 4-OH benzoic acid can be synthesized from phenol and CO₂ using a carboxylase enzyme in aqueous medium [26].

To reach stability and reusability of enzymes, many immobilization techniques have been developed. A very widely used technique is entrapment of the enzymes in a stabilizing matrix. In this field, Heichal-Segal et al. used an alginate-silicate sol-gel matrix to protect β-Glucosidase against thermal and chemical denaturation [27]. Immobilization of enzymes by physical adsorption has been reported by the groups of Kim et al. [28] and Lindgren et al. [29] who used microcrystalline cellulose and graphite respectively as adsorption matrices. Other Immobilization techniques include covalent attachment of enzymes to matrices and affinity immobilization, which is based on the specific interactions of the enzyme with its stabilizing matrix, which will be described in more detail below.

For CO₂ reduction, dehydrogenases are used. CO₂ reduction with dehydrogenases is already known from biological processes. The utilization of formate dehydrogenase in solution to reduce CO₂ to formate has first been reported already in 1976 by Ruschig et al. [30] and later by the group of Lu et al., who achieved an improvement concerning the enzyme stability by immobilizing formate dehydrogenase in an alginate-silica hybrid gel [31].

Furthermore, methanol production was achieved in a three step reaction with three dehydrogenases as reported by Obert et al. [32]. In each step, one molecule of the coenzyme nicotinamide adenine dinucleotide (NADH) is irreversibly oxidized and two electrons are consumed. In the first step of the reaction, CO₂ is reduced to formate, catalyzed by formate dehydrogenase. In the next step, formate is reduced to formaldehyde, catalyzed by formaldehyde dehydrogenase and in the last step, formaldehyde is reduced to methanol by alcohol dehydrogenase (see Figure 6) [32].

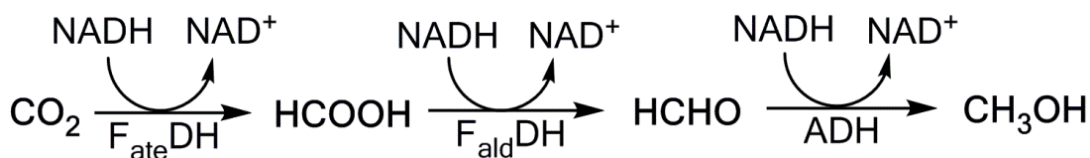


Figure 6: Enzyme-catalyzed reaction of CO₂ to methanol [32].

Dehydrogenases can effectively catalyze these reactions in presence of suitable electron donors which makes this CO₂ reduction feasible.

This work is focused on a combination of enzymatic- and electrochemical CO₂ reduction by using dehydrogenases as biocatalysts, which was already reported in 1994 by Kuwabata et al., who used formate dehydrogenase and methanol dehydrogenase, whereby methyl viologen or pyrroloquinolinequinone acted as electron mediators and glassy carbon was used as a working electrode in a CO₂ saturated phosphate buffer solution for formate and methanol production [33]. Further advances in this field were reached by the group of T. Reda et al., who report the reversible interconversion of CO₂ and formate by a formate dehydrogenase adsorbed to a pyrolytic graphite electrode [34].

In comparison to pure electrochemical CO₂ reduction, the biocatalyzed CO₂ reduction offers great selectivity, as enzymes catalyze only one specific reaction by binding only to specific substrates. Normally, an enzyme requires a cofactor, in this case nicotinamide adenine dinucleotide (NADH), which is irreversibly oxidized during the reaction and delivers two electrons to the enzyme. However, synthesis and regeneration of NADH is very expensive. Therefore the reason for using electrochemistry in this process is the purpose to replace the cofactor or other electron mediators required for an enzymatic reaction by providing the electrons directly from an electrode. This is realized by immobilizing the enzyme on an electrode surface as reported by S. Schlager et al. [35].

Using enzymatic catalysis to reduce CO₂ offers favorable advantages compared to using conventional catalysts. Enzyme catalysts are biocompatible and biodegradable, they show high chemoselectivity, regioselectivity, diastereoselectivity as well as enantioselectivity, which means that only the reaction to one selective product is catalyzed.

Furthermore, reactions can be performed under relatively mild conditions such as ambient temperature and pressure. In addition reactions can be carried out at low temperatures, physiological pH, and mostly in aqueous solution.

When dealing with enzymes, one has to consider several aspects concerning for example reaction parameters or solvents, which results in more difficult handling compared to the use of chemical catalysts. Most enzymes only operate proper if certain conditions with a defined pH range are provided. Moreover, aqueous solutions as reaction environment are preferred. Nevertheless, some enzymes also work in organic solvents. To keep the activity well enzymes should be stabilized in a matrix. The reason therefore is that every enzyme has a certain folding structure. If this structure is destroyed, either through mechanical forces, high temperatures, acids or organic solvents, the enzyme denatures and the function is lost. Sometimes denaturation is reversible, that is to say, the activity of the enzyme can return, but most of the time, the full activity of the enzyme cannot be regained. Enzymes can be protected against thermal and mechanical denaturation by immobilizing them. Immobilization of enzymes results in greater stability and lifetime of the enzymes and offers a way to reuse these biocatalysts. Thus, the processes can be designed more cost efficient. A great variety of enzyme immobilization methods have been reported in the past. Datta et al. present different immobilization techniques for enzymes [36].

A way to immobilize enzymes is by physical adsorption. In this method, only weak Van der Waals interactions, hydrophobic interactions and salt bridges are built up. For adsorption, either the support for enzyme immobilization is dipped into enzyme solution or the enzyme is dried on electrode surfaces. Appropriate materials are for example graphite [29], coconut fibers [37], mesoporous silica [38] or microcrystalline cellulose [28].

Another possibility for enzyme immobilization is realized by covalent attachment of the enzymes to a support. The covalent binding of an enzyme to supports occurs at the amino acid side chains, like arginine, aspartic acid or histidine. The reactivity is achieved by functional groups, e. g. imidazole, indolyl or hydroxyl. Using peptide modified supports enables higher specific activity, stability and a controlled protein orientation [39]. Cyanogen bromide modified agarose or sepharose containing a carbohydrate moiety and glutaraldehyde as

a spacer arm for covalent enzyme immobilization offer a way to make enzymes thermally stable [40].

Furthermore, affinity immobilization of enzymes can be done. This technique is based on the specificity of an enzyme with its support under different physiological conditions. This can be either done by precoupling the matrix to an affinity ligand for the desired enzyme or by conjugating an enzyme to an entity which develops an affinity to the matrix. Alkali stable chitosan-coated porous silica-beads [41] or agarose-linked multilayered concalavin A [42] are supports which can be used for affinity immobilization of enzymes.

Another method to immobilize enzymes is entrapment in a stabilizing matrix. The enzyme is caught by covalent or non-covalent bonds in the stabilizing matrix such as gels or fibers. There is a great variety of materials which can be used for encapsulation, for example alginate-gelatine-calcium hybrid carriers [43], alginate-silica hybrid gels [27], chitosan and chitin carriers [44]. Entrapment by nanostructured supports like electrospun nanofibers and pristine materials is also an attractive possibility for enzyme immobilization as it is easily reproducible and offers good mechanical stability [45]. Moreover, polypyrrole can be used as entrapment matrix for enzymes, reported by Swann et al. [46].

To conduct an enzymatic reaction successfully, the biological function of enzymes have to be understood. Therefore, informations about enzymes and enzymatic reactions will be discussed in more detail in the following.

Most enzymes consist of a proteinic backbone and an active site like a metal center. The primary structure of a protein corresponds to the sequence of covalently linked amino acids. Along the sequence globular, helical and sheet folds based on hydrogen bonding, resulting in the secondary structures, are formed. Tertiary structures are formed by the interactions of secondary structures like forming salt bridges and hydrophobic interactions. For every individual enzyme, this structure is specific and determines its activity. In some cases quaternary structures are formed by non-covalent interactions of multiple enzyme subunits (see Figure 7) [47].

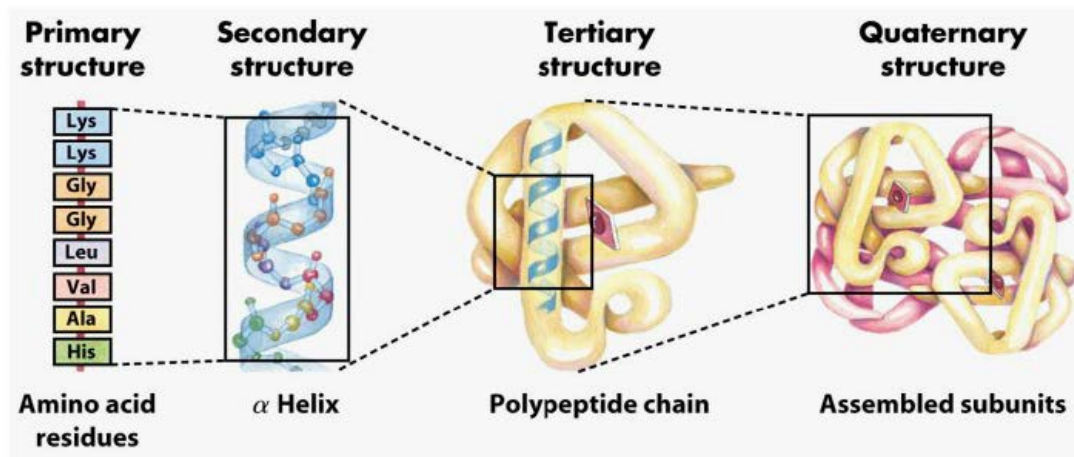


Figure 7: Three-dimensional structure of Enzymes: the primary structure corresponds to the sequence of the amino acids, the secondary structure is formed by hydrogen bonds along the sequence resulting in globular, helical and sheet folds and the tertiary structure results from interactions of the secondary structures. Quaternary structures can be formed by association of different protein units [47].

In many micro and macroorganisms enzymes play an important role. Enzymes are biocatalysts and are therefore responsible to enable and/or accelerate several reactions. Proteases and amylases are catalyzing reactions in the digestive system, kinases and phosphatases are important for signal transduction. An enzyme-catalyzed reaction takes place on a specific site of the enzyme, called the active site. The molecule binding to the active site is called the substrate. The active site contains amino acid residues which bind to the substrate and catalyze its reaction to the product. The enzyme-substrate complex was first mentioned by Adolphe Wurtz in 1880. He observed a precipitate during the papain-catalyzed hydrolysis of fibrin, of which he thought it was an enzyme-substrate complex acting as an intermediate in the hydrolysis [48].

Figure 8 shows a model of an enzyme catalyzed reaction. The substrate binds to the active site of the enzyme, which is specific for this substrate. By stabilizing the transition state, the enzyme lowers the activation energy and makes the reaction energetically more favorable. Then, the complex dissociates again into the free enzyme and the product. Without using an enzyme, the transition state, which is energetically unfavorable, is not stabilized so the activation energy is high.

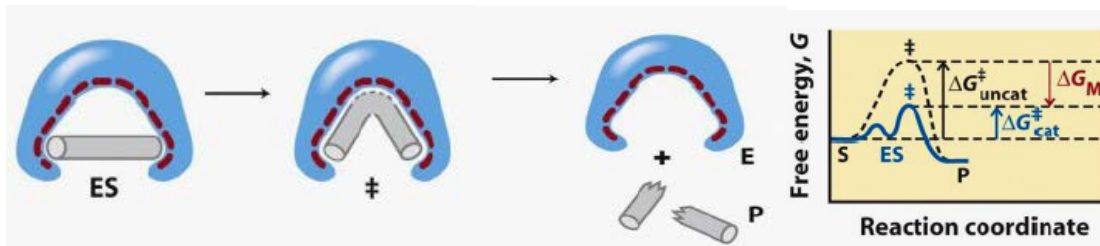


Figure 8: Principle of an enzyme-catalyzed reaction: The enzyme binds to a specific substrate, it stabilizes the energetically unfavorable transition state thereby lowering the activation energy of the reaction. Then, the specific product dissociates from the enzyme [47].

Enzymes do not affect the equilibrium of a certain reaction. They can only enhance the reaction rate by lowering the activation energy of the transition state.

Figure 9 compares the activation energy of an uncatalyzed (black) reaction with the activation energy of an enzyme-catalyzed (blue) reaction [47].

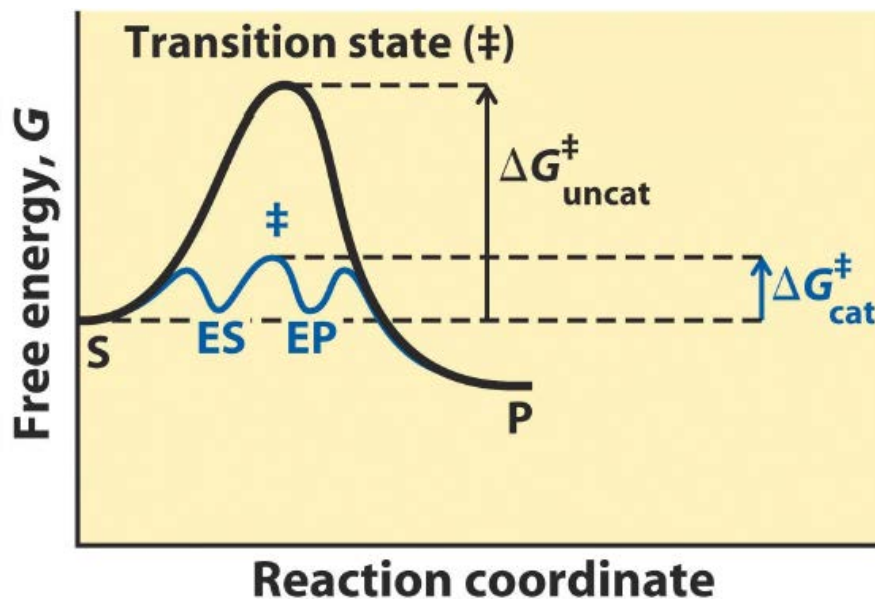


Figure 9: Comparison of energy diagrams of an enzyme-catalyzed reaction (blue curve) with an uncatalyzed reaction (black curve). It is apparent that the enzyme-catalyzed reaction has a much lower activation energy as opposed to the uncatalyzed reaction [47].

It is important in enzyme-catalyzed reactions to keep in mind the kinetics of the reactions. The limiting factor which affects the rate of an enzyme-catalyzed reaction is the concentration of substrate [S]. As substrate is needed to form the

enzyme-substrate complexes, enough substrate must be provided. However, at a certain concentration of substrate, the initial velocity V_0 of an enzymatic reaction does not increase anymore and a maximum velocity is reached. The dependence of the initial rate from different substrate concentrations is illustrated in Figure 10.

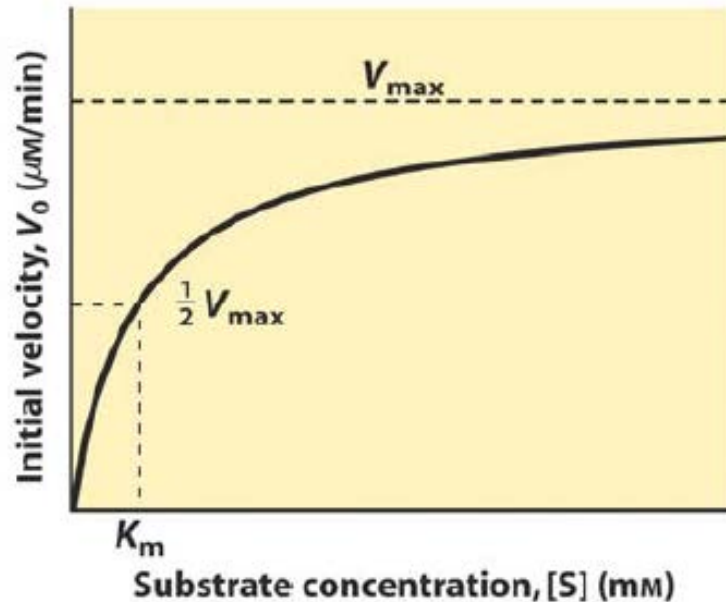


Figure 10: Dependence of initial velocity on substrate concentration: At low substrate concentrations $[S]$, there is an almost linear increase of the initial velocity V_0 with increasing $[S]$. At high $[S]$, however, V_0 does not rise any more, which means that the maximum velocity V_{max} is reached [47].

At low concentrations of substrate, the initial velocity increases almost linearly with increasing $[S]$. At high substrate concentrations, the increase in initial velocity in response to increasing $[S]$ gets smaller until V_0 does not rise anymore. This velocity is called the maximum velocity V_{max} . This plateau was first observed by Henri [49].

The kinetic model which was developed by L. Michaelis and M. Menten in 1913 provides an explanation of this effect. They propose that the enzyme and the substrate form an enzyme-substrate complex ES in a fast, reversible step. This complex breaks down in the slow second step into the free enzyme E and the product P (see Figure 11).

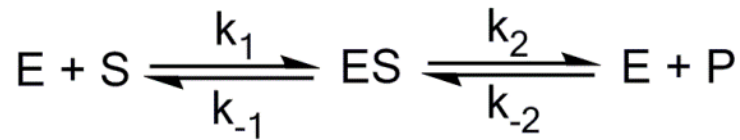


Figure 11: Reaction scheme of an enzyme-catalyzed reaction: The enzyme and the substrate are forming the Enzyme-Substrate complex, which is followed by the dissociation of the complex into free enzyme and the product.

The reaction rate is proportional to the concentration of ES, being the species which reacts in the slowest step. At low substrate concentration most of the enzyme is in its free form E. The reaction rate is proportional to the substrate concentration [S] as the equilibrium of the reaction is pushed to the formation of ES as [S] gets bigger.

The maximum initial rate is reached when all enzymes have already formed the ES complex, the enzyme is saturated with the substrate and further increase in substrate concentration does not affect the reaction rate any more, which can be seen in Figure 10.

The graph describing the relationship between [S] and the initial velocity of the reaction V_0 is similar for most enzymes, which can be mathematically described by the Michaelis-Menten equation (Equation 5) [47].

$$V_0 = \frac{V_{\max} [S]}{K_m + [S]} \quad (5)$$

[S]...Substrate concentration

V_0 ...Initial velocity

V_{\max} ...Maximum velocity

K_m ...Michaelis constant

2. Materials and Methods

In the first part, a carbonfelt (CF) electrode covered with an alginate layer modified with the three dehydrogenases was fabricated to produce methanol from a CO₂ saturated buffer-electrolyte solution. In preliminary experiments it has already been shown that this process was working for the first reaction step from CO₂ to formate.

In the second part, other electrode materials (Platinum, Graphite) and immobilization techniques were investigated for function, efficiency and stability. For this purpose, only the first step of CO₂ reduction to formate catalyzed by formate dehydrogenase was performed for simplicity and cost reasons.

2.1. Chemicals

Formate Dehydrogenase from *Candida boidinii* (F_{ate}DH) (lyophilized powder, 5.0 – 15.0 units / mg protein), Formate Dehydrogenase from *Candida boidinii*, (liquid (clear) ~ 50 u/ml), Formaldehyde Dehydrogenase, from *Pseudomonas* sp., (F_{ald}DH) (lyophilized powder, 1.0 – 6.0 units / mg solid), Alcohol Dehydrogenase, from *Saccharomyces cerevisiae* (ADH) (activity ≥ 300 units / mg protein), Alginic acid sodium salt, from brown algae (Alginate), Tetramethylorthosilicate, reagent grade, 98 % (TEOS), Pyrrole, reagent grade, 98 % and Tetrabutylammoniumhexafluorophosphate (TBAPF₆) were purchased from Sigma Aldrich.

Trizma[®] base, also purchased from Sigma Aldrich, was used to prepare 0.05 M buffer solution which was adapted to pH 7.64 with HCl.

All chemicals were used as received.

2.2. Apparatus

Electrochemical measurements were carried out on a Jaissle Potentiostat-Galvanostat IMP 88 PC-100. Formate was detected on an ICS-5000 Dionex-DC Capillary Ion Chromatograph with an IonPac[®] AS19 Analytical Column from Thermo Scientific. Methanol was detected on a TRACE 1310 Gas Chromatograph from Thermo Scientific. Microscopic Measurements were done with Nikon ECLIPSE LV 100 ND optical microscope.

For electrochemical measurements, a standard three electrode system with separate cathodic and anodic chambers (two compartment cell) shown in Figure 12 was used. For electropolymerisation of pyrrole, a one compartment setup was used.

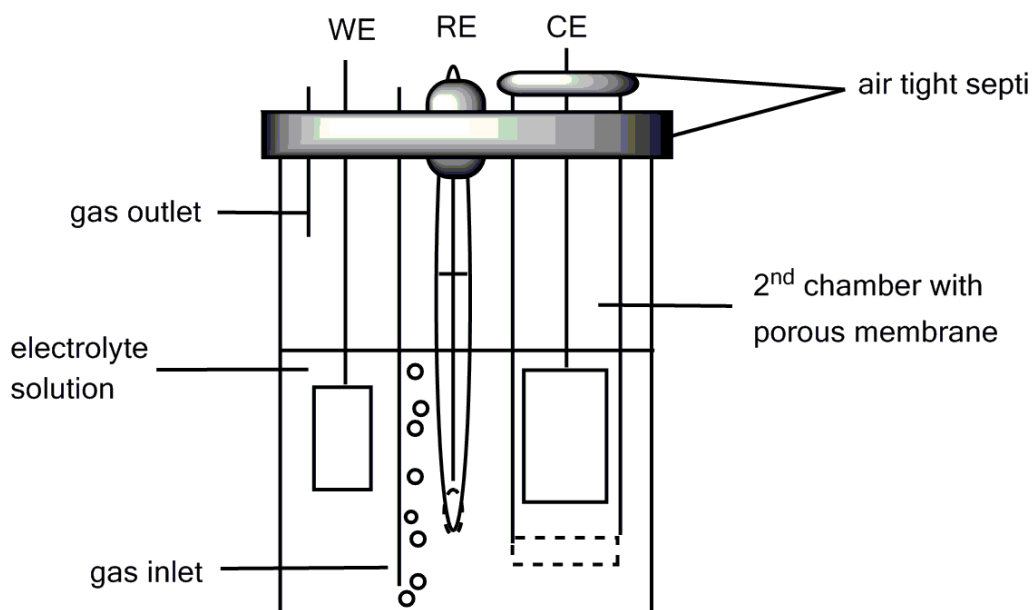


Figure 12: Experimental setup: electrochemical two compartment cell with different enzyme- modified electrodes as working electrodes (WE), platinum foil as counter electrode (CE) and Ag/AgCl/3M KCl as reference electrode (RE). 0.05 M Trizma[®]buffer, pH adjusted to 7.64 with HCl is used as electrolyte solution.

2.3. CF/Alginate/ $F_{ate}DH$ / $F_{ald}DH$ /ADH – Electrodes

2.3.1. Fabrication of CF/Alginate/ $F_{ate}DH$ / $F_{ald}DH$ /ADH-Electrodes

The alginate suspension for immobilizing the enzymes was prepared as reported from the group of Lu et al. [31]. 0.2 g Alginic Acid Sodium Salt, 1.0 mL Tetraethyl orthosilicate (TEOS) and 3.0 ml 18 M Ω water were mixed to a homogeneous suspension. About 5 mg of $F_{ate}DH$, Formaldehyde Dehydrogenase ($F_{ald}DH$) and Alcohol Dehydrogenase (ADH) were dissolved in 1 ml 0.05 M TRIS-HCl, pH 7.64 and added to the suspension. A carbonfelt (CF) Electrode of about 7.5 cm² surface was soaked in the enzyme suspension for 2-3 min and subsequently dipped in 0.2 M CaCl₂ for 30 min to achieve conglomeration. In Figure 13, a CF/Alginate electrode containing three different dehydrogenases is shown.



Figure 13: Carbonfelt Electrode covered with Enzyme - Alginate layer.

2.3.2. Characterization of CF/Alginate/ $F_{ate}DH/F_{ald}DH/ADH$ -Electrodes

The characterization of the CF/Alginate/ $F_{ate}DH/F_{ald}DH/ADH$ Electrode was performed with a three electrode setup shown in Figure 12. Platinum foil was used as a counter electrode. 0.05 M TRIS-HCl, pH 7.64 served as electrolyte. To remove oxygen, the system was purged with N_2 . The electrode was cycled between 0.3 V and - 1.6 V vs. a Ag/AgCl reference electrode with a scan rate of 50 mV/s. Characterization was repeated in a CO_2 purged system to investigate the CO_2 reduction ability of the electrode. For saturation, purging times of about 15 min were chosen.

2.3.3. Electrolysis with CF/Alginate/ $F_{ate}DH/F_{ald}DH/ADH$ -Electrodes

Electrolysis was carried out at -1.2 V and -1.6 V for 1.5 h after the system had been purged for 30 min with CO_2 . Samples taken before and after electrolysis were analyzed by Liquid Gas Chromatography for methanol analysis. For reference measurements, electrolysis was done with CF/Alginate electrodes without enzymes and with a blank carbonfelt electrode.

2.4. Pt/PPy/Alginate/ $F_{ate}DH$ – Electrodes

2.4.1. Fabrication of Pt/PPy/Alginate/ $F_{ate}DH$ -Electrodes

Pyrrole was electropolymerised potentiodynamically on a platinum electrode. Platinum foil was used as counter electrode and Ag wire coated with AgCl as

quasi-reference electrode. 625 μ L Pyrrole monomer and 18 mL 0.1 M Tetrabutylammoniumhexafluorophosphate (TBAPF₆) in acetonitrile served as polymerisation solution. The system was scanned between 0.9 V and -0.8 V with 100 mV/s for the duration of 70 cycles. The fabricated Pt/Polypyrrole (PPy) electrode was entirely coated with Alginate/F_{ate}DH suspension produced as indicated in **2.3.1.** and dipped in 0.2 M CaCl₂ for 30 min.

Figure 14 depicts a Pt/PPy/Alginate/F_{ate}DH electrode.



Figure 14: Platinum Electrode covered with a film of polypyrrole and an Alginate - Enzyme layer.

2.4.2. Characterization of Pt/PPy/Alginate/F_{ate}DH Electrodes

The characterization of the Pt/PPy/Alginate/F_{ate}DH Electrode was performed as mentioned in **2.3.2.**

The electrode was cycled between 0.3 V and -1.8 V vs. Ag/AgCl.

2.4.3. Electrolysis with Pt/PPy/Alginate/F_{ate}DH Electrodes

Electrolysis was performed at -1.6 V for 1.5 h after the system had been purged for 30 min with CO₂. Furthermore, electrolysis was done at -1.4 V. Samples taken before and after electrolysis were analyzed by Capillary Ion

Chromatography for formate analysis. For reference measurements, electrolysis was done with a Pt/PPy/Alginate electrode without enzyme.

2.5. Pt/PPy/F_{ate}DH – Electrodes

2.5.1. Fabrication of Pt/PPy/F_{ate}DH - Electrodes

The electrodes were made as reported by Swann et al. [46]. The platinum electrodes were cleaned by flaming and afterwards cycled between -0.2 V and + 1.2 V in nitrogen bubbled 0.5 M aqueous H₂SO₄. The cleaned electrode was rinsed with 18 MΩ water. Then the electrode was dipped in 2-3 mg / mL F_{ate}DH solution and immediately after immersion (1 – 2 s) the adsorption potential of + 0.5 V vs. Ag/AgCl was applied for 10 min. Within 20 s after adsorption, the electrode was transferred into the polymerisation solution (0.1 M pyrrole, 0.1 M KCl, pH 3) and the polymerisation potential of + 0.7 V was applied for 60 s for potentiostatic electropolymerisation. After polymerisation the electrode was rinsed with 18 MΩ water.

In Figure 15, a picture of the Pt/PPy/F_{ate}DH electrode is shown.



Figure 15: Platinum electrode covered with a thin layer of polypyrrole with incorporated enzyme.

2.5.2. Characterization of Pt/PPy/F_{ate}DH - Electrodes

The characterization of the Pt/PPy/F_{ate}DH Electrode was performed as mentioned in 2.3.2. The electrodes were cycled between + 0.3 V and -1.8 V vs. Ag/AgCl.

2.5.3. Electrolysis with Pt/PPy/ $F_{ate}DH$ - Electrodes

Electrolysis was carried out as described in 2.2. A voltage of -1.8 V was applied for a duration of 2 h. Furthermore, electrolysis at -1.4 V was investigated.

Samples taken before and after electrolysis were analyzed by capillary ion chromatography for formate analysis.

For reference measurements electrolysis with Pt/PPy electrodes without enzyme was conducted.

2.6. Physical Adsorption of $F_{ate}DH$ on Graphite Rods

2.6.1. Production of Graphite/ $F_{ate}DH$ Electrodes

$F_{ate}DH$ was immobilized on Graphite rods according to Lindgren et al. [29]. Graphite with about 2.9 cm² surface area was polished with wet fine emery paper and then sonicated for 30 s to remove excess graphite particles. Afterwards, the electrode was dried with a paper towel and 10 mg $F_{ate}DH$ dissolved in 40 μ L 0.05 M Tris-HCl buffer, pH 7.64 was dropped on the graphite surface. After 30 min drying at room temperature, the electrode was transferred into a glass beaker, covered with sealing film and stored for 2 h at 4 °C to allow the immobilization proceed. Then, the electrode was rinsed with 18 M Ω Water.

Furthermore, following modifications of the given procedure were investigated:

- $F_{ate}DH$ solution was dropped onto the graphite surface. Afterwards the electrode was kept in the solution for 20 min, dried for 30 min at room temperature. Additionally, the graphite surface was not polished before adsorption.

- The adsorption was carried out 2 h at room temperature, while the electrode was still kept in the $F_{ate}DH$ solution. Subsequently, the electrode was dried overnight at room temperature in a desiccator over silica gel.

The rest of the process was in both cases performed as stated by Lindgren et al. [29].

- The immobilization process was carried out by using 0.4 mL $F_{ate}DH$, liquid (clear), ~ 50 u/ml instead of the lyophilized powder.

2.6.2. Characterization of Graphite/ $F_{ate}DH$ Electrodes

Characterization of the Graphite/ F_{ate} DH electrodes was carried out as described in 2.3.2. The electrodes were cycled between 0.3 V and – 1.4 V vs. Ag/AgCl.

2.6.3. Electrolysis with Graphite/ F_{ate} DH Electrodes

After the system had been purged for 30 min with CO₂, a voltage of – 1.4 V was applied for 1.5 h. Furthermore, electrolysis was performed at – 1.0 V for 1.5 h. Samples taken before and after electrolysis were analyzed by Capillary Ion Chromatography for formate analysis. For reference measurements, electrolysis with a blank graphite rod was carried out.

3. Results and Discussion

3.1. CF/Alginate/ F_{ate} DH/ F_{ald} DH/ADH – Electrodes

3.1.1. Characterization of CF/Alginate/ F_{ate} DH/ F_{ald} DH/ADH electrodes

Cyclic voltammograms (CV) of carbonfelt electrodes modified with an alginate layer containing three different dehydrogenases (CF/Alginate/ F_{ate} DH/ F_{ald} DH/ADH) were recorded at different negative sweeping potentials to figure out the most suitable one for CO₂ reduction to methanol. Potentials of -0.6 V, -1.2 V and -1.6 V vs. Ag/AgCl were examined.

Figure 16 and Figure 17 show the CVs of a CF/Alginate/ F_{ate} DH/ F_{ald} DH/ADH electrode recorded in a N₂ purged system and in a CO₂ purged system at negative sweeping potentials of -1.2 V and -1.6 V. The black curves depict the CV recorded in a N₂ purged system, the red curves show the CV recorded in a CO₂ purged system. The reductive current for CO₂ reduction starts to increase at about -0.4 V. At -1.2 V an increase in the reductive current of about 0.3 mA for the CO₂ purged system in comparison to the N₂ purged system is observed. Comparison of CVs at -1.2 V and -1.6 V shows the same difference in current density between curves of the N₂ and curves of the CO₂ purged systems. However, the current densities are more than four times higher for the CVs with a negative sweep potential of -1.6V.

Further, CVs were recorded for another negative sweeping potential of -0.6 V, which, however do only show a slight increase in reductive current for CO₂ reduction and small current densities not sufficient for methanol production. From the theoretical point of view, CO₂ reduction to methanol occurs at -0.38 V vs. NHE, which is about -0.6 V vs. Ag/AgCl. For CO₂ reduction at the

CF/Alginate/ $F_{ate}DH/F_{ald}DH/ADH$ electrode obviously a significant overpotential is required, which is due to a low conductivity of the alginate layer. Moreover, it is assumed that the thickness of the alginate layer also influences CO_2 reduction.

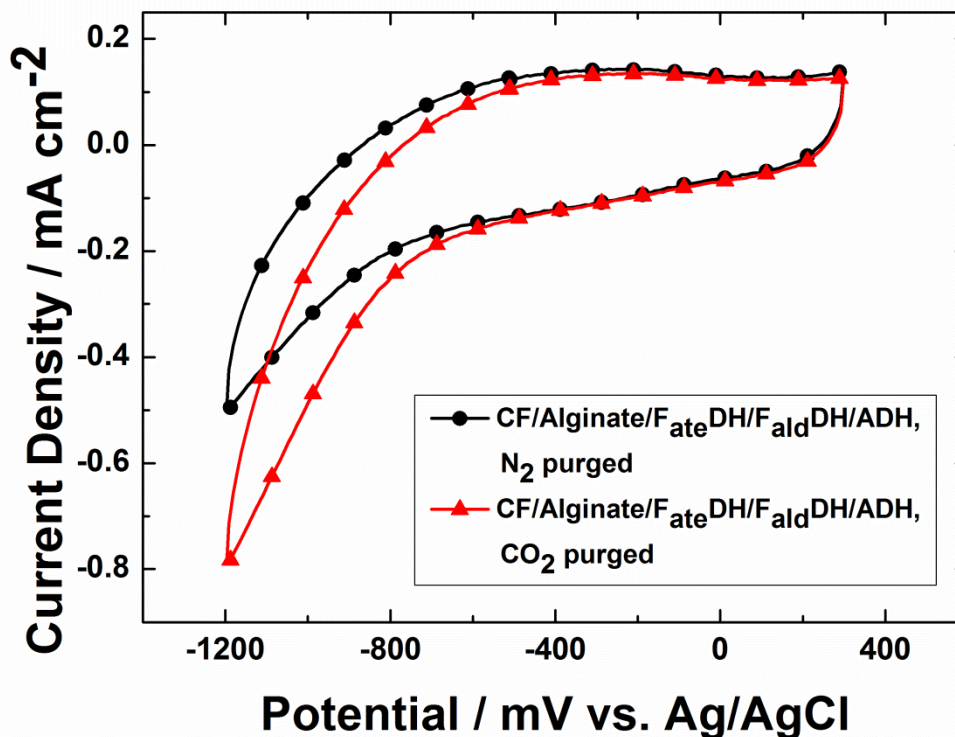


Figure 16: CVs of a CF/Alginate/ $F_{ate}DH/F_{ald}DH/ADH$ electrode. Comparison of the CV recorded in the N₂ purged system (black curve) to the CV recorded in the CO₂ purged system (red curve) with increase in reductive current for the CO₂ purged system starting at about -0.6 V.

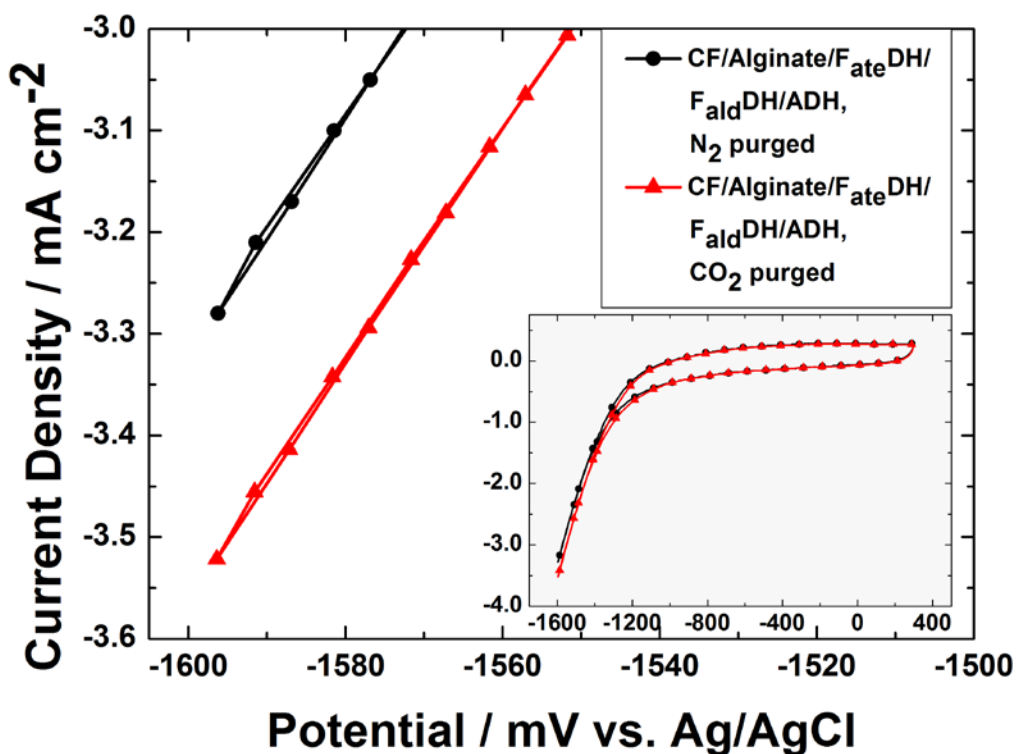


Figure 17: CVs of a CF/Alginate/F_{ate}DH/F_{alid}DH/ADH electrode at a negative sweeping potential of -1.6 V. The black curve shows the CV of the N₂ purged system, the red curve displays the CV recorded in a CO₂ purged system. The increase in reductive current for the CO₂ purged system starts at about -1.2 V.

Figure 18 shows the CVs of a pristine CF/Alginate electrode without enzyme modification in N₂ and CO₂ saturated systems. For this electrode, an increase in reductive current for the CO₂ purged system can be observed as well. However, methanol production was only observed for CO₂ reduction using enzyme modified electrodes. We assume that the increase in reductive current using the pristine electrode is attributed to side reactions, such as water splitting, as there is also an increase after N₂ purging.

From the CVs above the potentials for the electrolysis experiments was set at -1.2 V and -1.6 V. Electrolysis at the lower potential of -1.2 V is favored due to avoidance of side reactions and therefore concerning faradaic efficiency of methanol production.

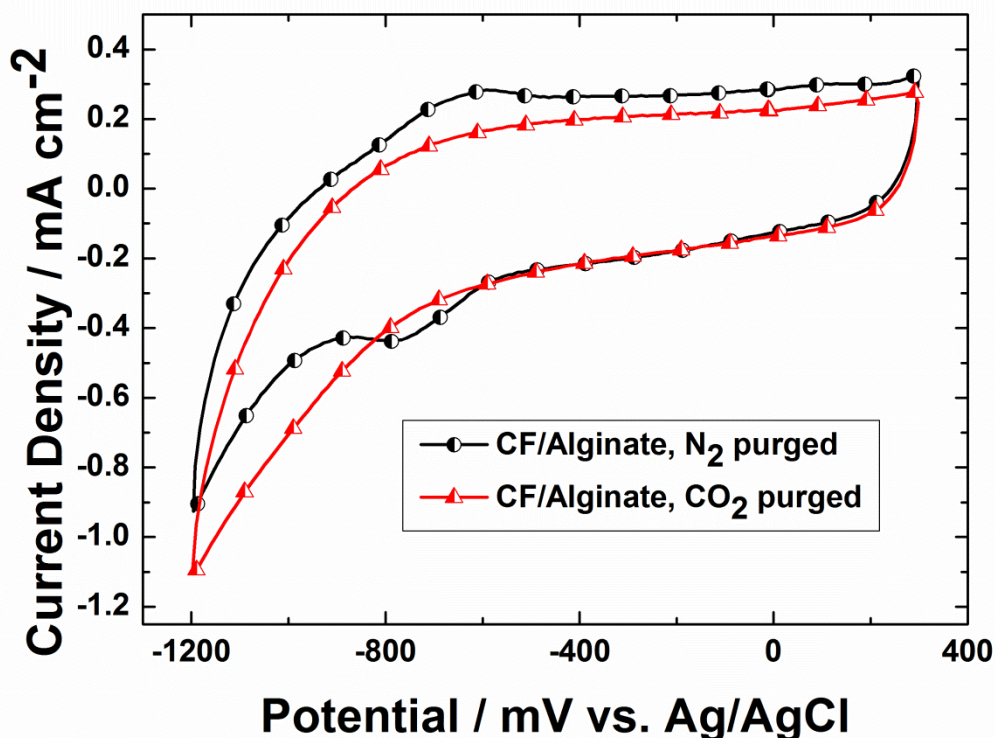


Figure 18: CVs of a CF/Alginate electrode without enzyme modification recorded in a N₂ purged system (black curve) and in a CO₂ purged system (red curve) at a negative sweeping potential of -1.2 V vs. Ag/AgCl. There is an increase in reductive current for the CV measured in the CO₂ purged system relative to the CV measured in the N₂ purged system.

In Figure 19 the CVs of a blank CF electrode recorded in a N₂ purged system and a CO₂ purged system, respectively, at a negative sweeping potential of -1.2 V are compared. The current densities of the CVs of the blank CF electrode are in a similar range as in the CVs of the CF/Alginate/F_{ate}DH/F_{ald}DH/ADH electrode (see Figure 16). An increase in reductive current for the N₂ purged system and an even slightly higher reductive current for the CO₂ purged system is observed. However, as for CF/Alginate electrodes, no methanol could be detected, indicating that other CO₂ reduction reactions, which were not investigated in this work, are occurring at this electrode at this potential.

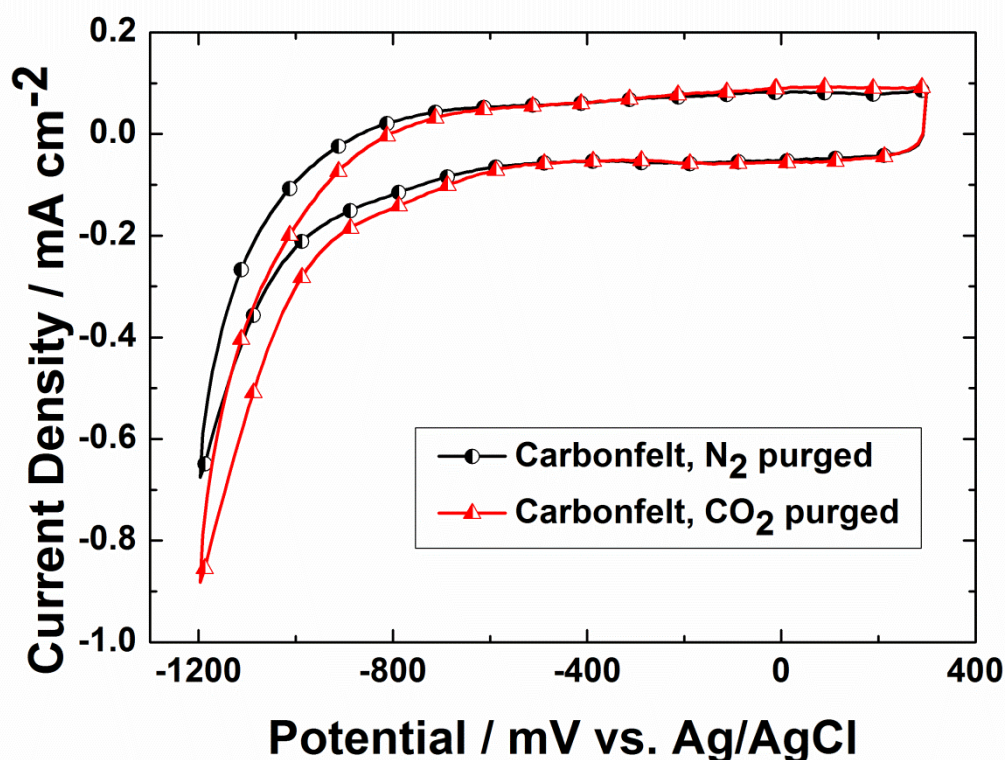


Figure 19: Comparison of CVs of a blank CF electrode at a negative sweeping potential of -1.2 V vs. Ag/AgCl. The black curve shows the N₂ purged system, the red curve shows the CO₂ purged system. An increase in reductive current for the CO₂ purged system can be seen.

Electrolysis with the CF/Alginate/F_{ate}DH/F_{ald}DH/ADH electrode at -1.2 V yielded 0.12 mmol/L methanol. Electrolysis experiments using CF and CF/Alginate electrodes, carried out for reference, did not deliver methanol, as reported above.

3.1.2. Electrolysis with CF/Alginate/F_{ate}DH/F_{ald}DH/ADH electrodes

Figure 20 depicts the current-time curves which were recorded during electrolysis at -1.6 V with a CF/Alginate/F_{ate}DH/F_{ald}DH/ADH electrode and with electrodes without enzyme modification. The assumption was made, that the enzymes in the CO₂ purged system result in a suppression of water splitting and therefore enable high faradaic efficiency, which will be discussed below. However, the current-time curves of the enzyme modified electrode shown in Figure 20 cannot be used to reinforce this presumption, as the carbonfelt was not fully coated with alginate-enzyme gel therefore allowing water splitting to occur more dominantly. It can be seen that the current of the blank carbonfelt electrode and of the CF/Alginate electrode are much lower than the current of

the enzyme modified electrode. The current-time curve of the enzyme modified electrode depicted in Figure 21 shows a much lower current flowing during electrolysis, and presumably most of the current was used for methanol production and only little water splitting was occurring.

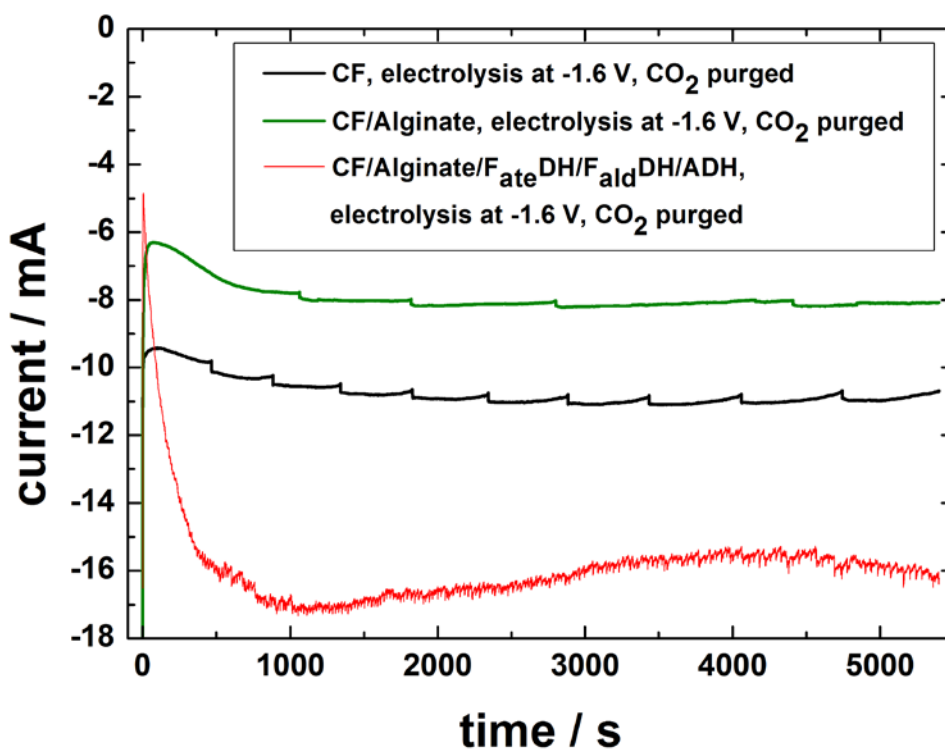


Figure 20: Current-time curves of a CF/Alginate/F_{ate}DH/F_{ald}DH/ADH and a blank carbonfelt electrode as well as of a CF/Alginate electrode. The current of the enzyme modified electrode is much higher than the current of the blank electrodes because the enzyme modified electrode was not fully covered with alginate gel thereby allowing more water splitting.

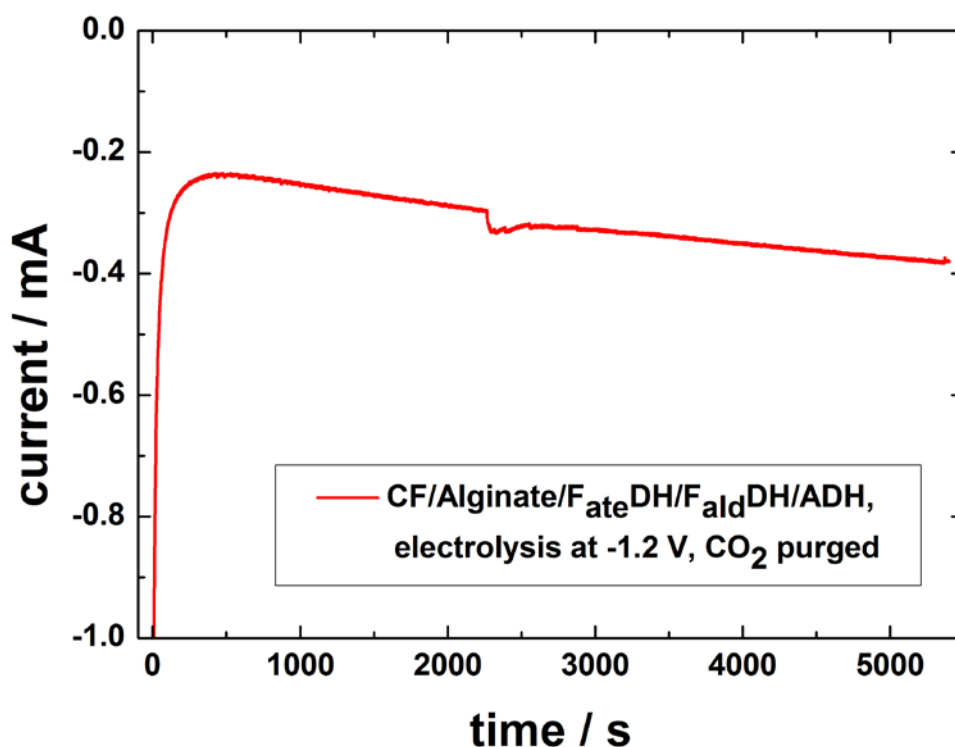


Figure 21: Current-time curve of a CF/Alginate/F_{ate}DH/F_{ald}DH/ADH electrode recorded during electrolysis at -1.2 V in a CO₂ purged system.

In Figure 22, the gas chromatograms of the electrolyte solutions after electrolysis with the CF/Alginate/F_{ate}DH/F_{ald}DH/ADH electrode at -1.2 V and -1.6 V are shown.

The peak at 2.06 min was identified as methanol by external standard calibration. The methanol peak is growing with higher potential used for electrolysis. The peak close to the retention time of methanol at 2.02 min is attributed to a side product which could not be identified yet.

During 1.5 h electrolysis at -1.2 V, 0.12 mmol/L methanol, corresponding to a faradaic efficiency of about 90% were produced. The potential of -1.2 V is favored for electrolysis because at higher negative potentials the increase of current density for CO₂ reduction is not higher. (See Figure 16 and Figure 17) Electrolysis was further investigated at -1.6 V, where water splitting occurred at a higher rate, which resulted in very low faradaic efficiency of about 6% compared to electrolysis at -1.2 V. Further, electrolysis was carried out with a CF/Alginate electrode without enzyme modification and with a blank CF electrode for reference measurements. Nevertheless, methanol was only detected after electrolysis with the enzyme-modified electrode.

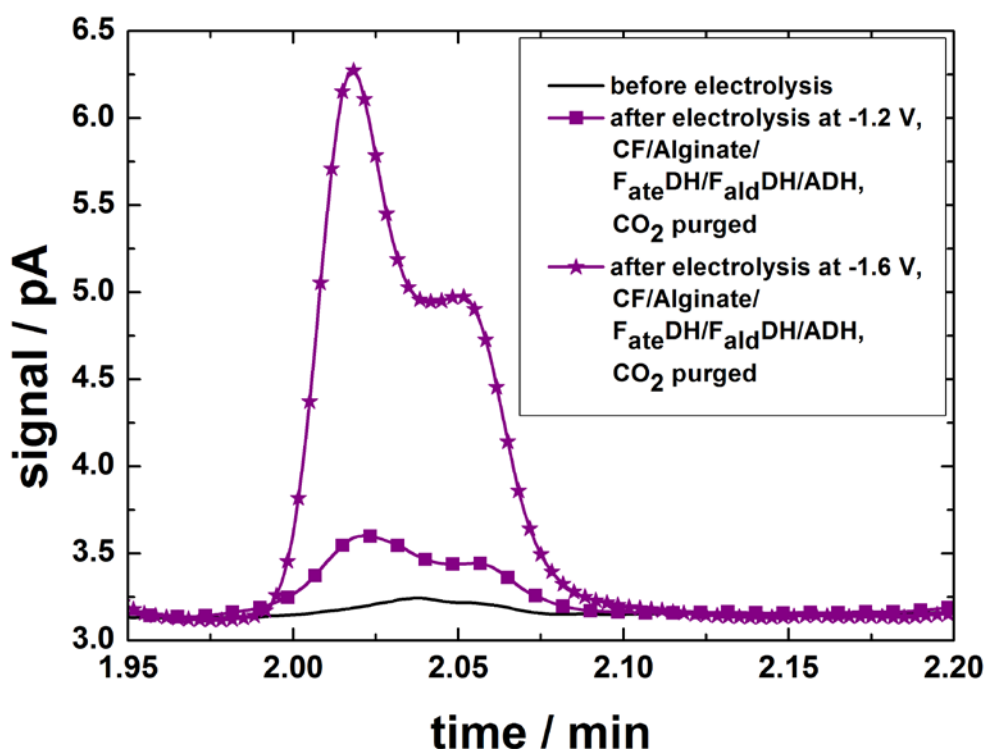


Figure 22: Gas chromatogram of the electrolyte solutions after electrolysis at -1.2 V and at -1.6 V for 1.5 h. Methanol elutes at 2.06 min. The methanol peak is growing with higher potential used for electrolysis. The peak at 2.02 min is attributed to a side product and could not be identified yet.

Figure 23 show the gas chromatogram of the electrolyte solution after electrolysis at -1.6 V with a blank CF/Alginate electrode without enzyme modification conducted for reference. It can be seen that the methanol peak does not grow after electrolysis with the electrode without enzyme modification, so no methanol was produced with this blank electrode. There is already a methanol peak before electrolysis because methanol was still on the chromatography column from measurements before.

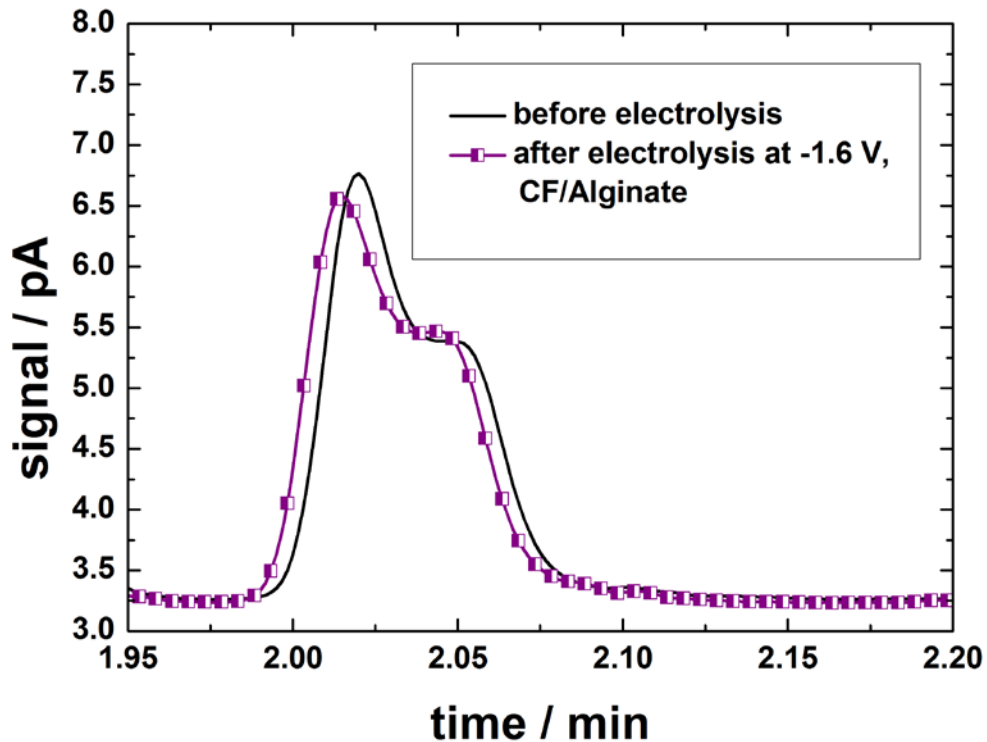


Figure 23: Gas chromatogram recorded after electrolysis at -1.6 V with a CF/Alginate electrode without enzyme modification. The peak at 2.06 min, corresponding to methanol, has not grown during electrolysis. The reason for the peak which is present is that there was still methanol on the chromatography column from measurements before.

3.1.3. Faradaic efficiency of Methanol production at CF/Alginate/ $F_{ate}DH/F_{ald}DH/ADH$ electrodes

Duration of Electrolysis: 1.5 h = 5400 s

Mean electric current flow during electrolysis: $- 2.96 \cdot 10^{-4}$ A

The amount of charge is defined by the product of electric current and time of electrolysis:

$$Q = I \cdot t = 2.96 \cdot 10^{-4} \text{ A} \cdot 5400 \text{ s} = 1.60 \text{ A s} = 1.60 \text{ C} \quad (10)$$

Q...amount of charge[C]

I...electric current [A]

t...time [s]

The number of moles provided for the reaction can be calculated by dividing the charges with the faradaic constant $F = 96485 \text{ C/mol}$

$$X = \frac{Q}{F} = \frac{1.6 \text{ C}}{96485 \frac{\text{C}}{\text{mol}}} = 1.66 \cdot 10^{-5} \text{ moles of electrons} \quad (11)$$

According to the reaction equation for CO₂ reduction to methanol, the production of each mole of Methanol requires six electrons:



$$n_{\text{th}} = \frac{1.66 \cdot 10^{-5} \text{ moles of electrons}}{6 \text{ e}^-} = 2.76 \cdot 10^{-6} \text{ moles} \quad (13)$$

n_{th} ...theoretical amount of methanol [mol]

By dividing the practical amount of methanol by the theoretical maximum amount, the faradaic efficiency η_F is obtained:

$$\eta_F = \frac{n_{\text{MeOH}}}{n_{\text{th}}} = \frac{2.4 \cdot 10^{-6} \text{ mol}}{2.8 \cdot 10^{-6} \text{ mol}} = 86 \% \quad (14)$$

η_F ...faradaic efficiency [-]

n_{MeOH} ...produced amount of methanol [mol]

n_{th} ...theoretically achievable amount of methanol [mol]

3.1.4. Stability of CF/Alginate/*F_{ate}DH*/*F_{ald}DH*/ADH electrodes

After storing the electrode for 3 weeks in 18 MΩ water, mechanical stability was still preserved. Longer storage times lead to softening of the alginate layer on the electrode. The comparison of the picture of the electrode when it has been stored for 3 weeks in 18 MΩ water shown in Figure 24 with the picture taken after a longer storage time of 4 weeks which is depicted in Figure 25, shows that the alginate layer already started to soften and swell up on the when the electrode had been stored for 4 weeks, while at a storage time of 3 weeks, the alginate layer was still quite tight.



Figure 24: CF/Alginate/ $F_{ate}DH$ / $F_{ald}DH$ /ADH electrode after 3 weeks storage in 18 M Ω water.



Figure 25: CF/Alginate/ $F_{ate}DH$ / $F_{ald}DH$ /ADH electrode after 4 weeks storage in 18 M Ω water.

3.2. Pt/PPy/Alginate/ $F_{ate}DH$ Electrodes

3.2.1. Characterization of Pt/PPy/ $F_{ate}DH$ electrodes

The platinum electrode covered with a polypyrrole film and an alginate layer modified with $F_{ate}DH$ (Pt/PPy/Alginate/ $F_{ate}DH$) was characterized by recording CVs at negative sweeping potentials of -1.4 V, -1.6 V and -1.8 V vs. Ag/AgCl to find out the optimal potential for CO₂ reduction to formate.

Figure 26 and Figure 27 display the CVs of a Pt/PPy/Alginate/ $F_{ate}DH$ electrode recorded in a N₂ purged system (black curve) and in a CO₂ purged system (red

curve) at negative sweeping potentials of -1.4 V and -1.6 V. At -1.4 V, the reductive current of the CO₂ purged system is about 0.15 mA higher than the current in the N₂ purged system. However, at -1.6 V the increase in current for the reduction of CO₂ is even higher with more than 0.4 mA, which is why this should be a decent potential for CO₂ reduction to formate.

In both CVs, the reductive current for the CO₂ purged system relative to the N₂ purged system starts to increase at about -1.1 V.

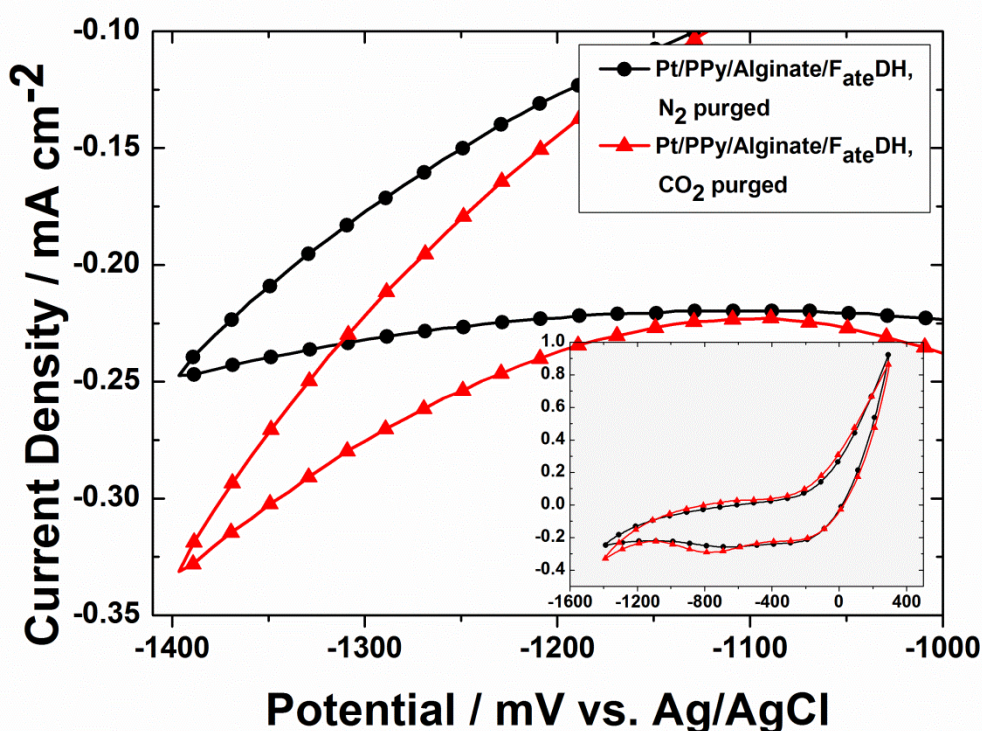


Figure 26: CVs of a Pt/PPy/Alginate/F_{ate}DH electrode at a negative sweeping potential of -1.4 V vs. Ag/AgCl. Comparison of the CVs recorded in the N₂ purged system (black curve) and in the CO₂ purged system (red curve) with increase in reductive current for the CO₂ purged system at -1.1 V.

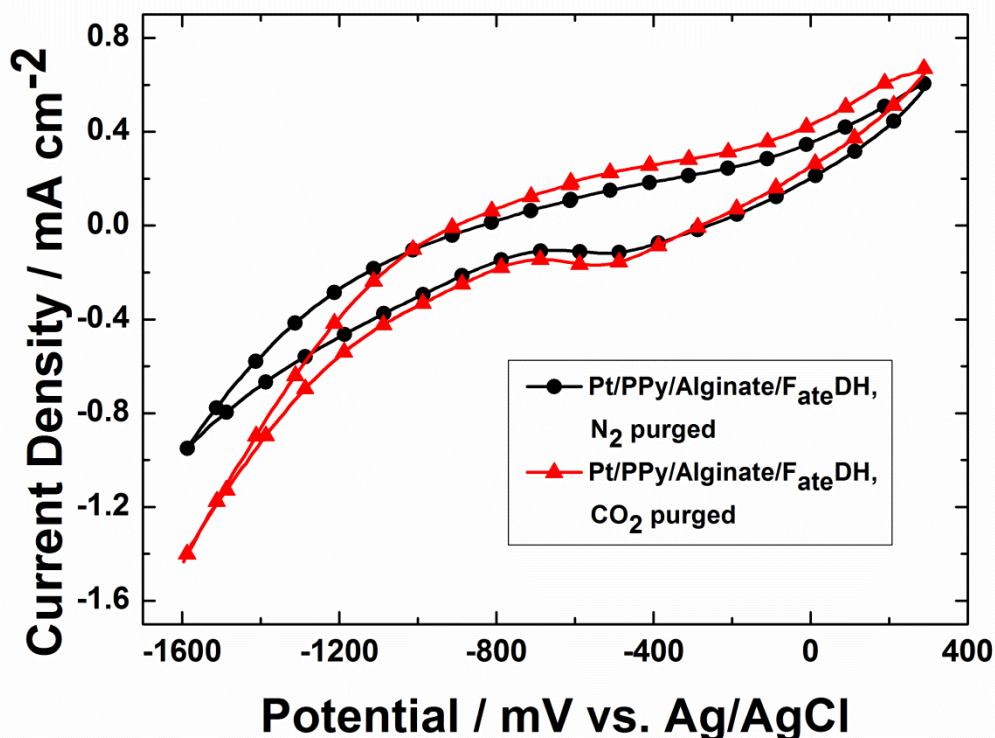


Figure 27: CVs of a Pt/PPy/Alginate/F_{ate}DH electrode at a negative sweeping potential of -1.6 V vs. Ag/AgCl. The CVs measured in the N₂ purged system (black curve) and the CVs recorded in the CO₂ purged system (red curve) are compared. A significant increase in reductive current for the CO₂ purged system can be seen starting at about -1.1 V.

The characterization of the Pt/PPy/Alginate/F_{ate}DH to a negative sweeping potential of -1.8 V did not result in a higher difference in reductive current between CVs recorded in N₂ and CO₂ purged system, compared to other potentials.

In Figure 28 the CVs of a Pt/PPy/Alginate electrode without enzyme modification are depicted. It is apparent that there is a small increase in reductive current in the CV recorded in the CO₂ purged system in comparison to the CV recorded in the N₂ purged system. This is presumably because of other CO₂ reduction reactions catalyzed by the electrode, which were, however, not investigated in this work, as reported above.

When the CVs of the electrode with formate dehydrogenase modification (see Figure 27) are compared to the CVs of the blank electrode shown in Figure 28, it is obvious, that the difference in reductive current is about four times higher for the system with enzyme modification.

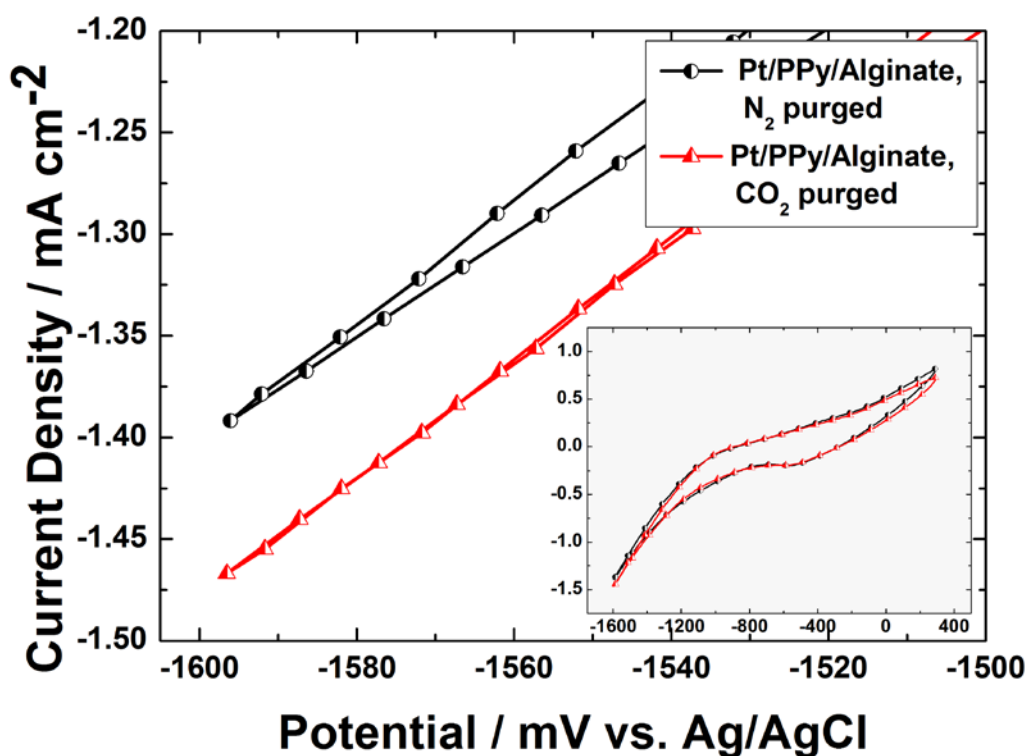


Figure 28: CVs of a platinum electrode modified with a polypyrrole film and an alginate layer without enzyme at a negative sweeping potential of -1.6 V. Comparison of CVs of the N₂ purged system (black curve) with the CO₂ purged system (red curve). A small increase in reductive current for the CO₂ purged system can be seen.

Electrolysis experiments with a Pt/PPy/Alginate/F_{ate}DH electrode at -1.6 V delivered 0.44 mmol/L formate. After electrolysis at lower or higher potentials, no formate could be detected in spite of the reductive current for the CO₂ purged systems which can be seen in the CVs. Further, significant amounts of formate could not be detected after electrolysis with electrodes without enzyme modification carried out for reference.

In theory, the potential for CO₂ reduction to formate is -0.61 V vs. NHE, which is about -0.8 V vs. Ag/AgCl. However, the potential used for electrolysis is much higher, because electrolytic resistance and resistance of the alginate layer have to be taken into account. The overpotential is even higher when using Pt/PPy/Alginate/F_{ate}DH electrodes as opposed to the CF/Alginate/F_{ate}DH/F_{ald}DH/ADH electrodes as the alginate layer is thicker and the surface area is not as big as in the case of carbonfelt.

3.2.2. Electrolysis with Pt/PPy/Alginate/ $F_{ate}DH$ electrodes

In Figure 29 the current-time curves recorded during electrolysis at -1.6 V with a Pt/PPy/Alginate/ $F_{ate}DH$ electrode and a Pt/PPy/Alginate electrode without enzyme modification are shown. These curves encourage the assumption that the enzymes are suppressing the side reaction of water splitting and allowing a high faradaic efficiency for this process. It is apparent that during electrolysis with the enzyme modified electrode less current is flowing compared to the electrolysis with the blank electrode. Therefore, in case of the enzyme modified electrode, mostly the enzyme catalyzed CO_2 reduction to methanol is occurring obviously and most of the current is used for this specific reduction, whereas with the blank electrode more water splitting occurs and no methanol is produced.

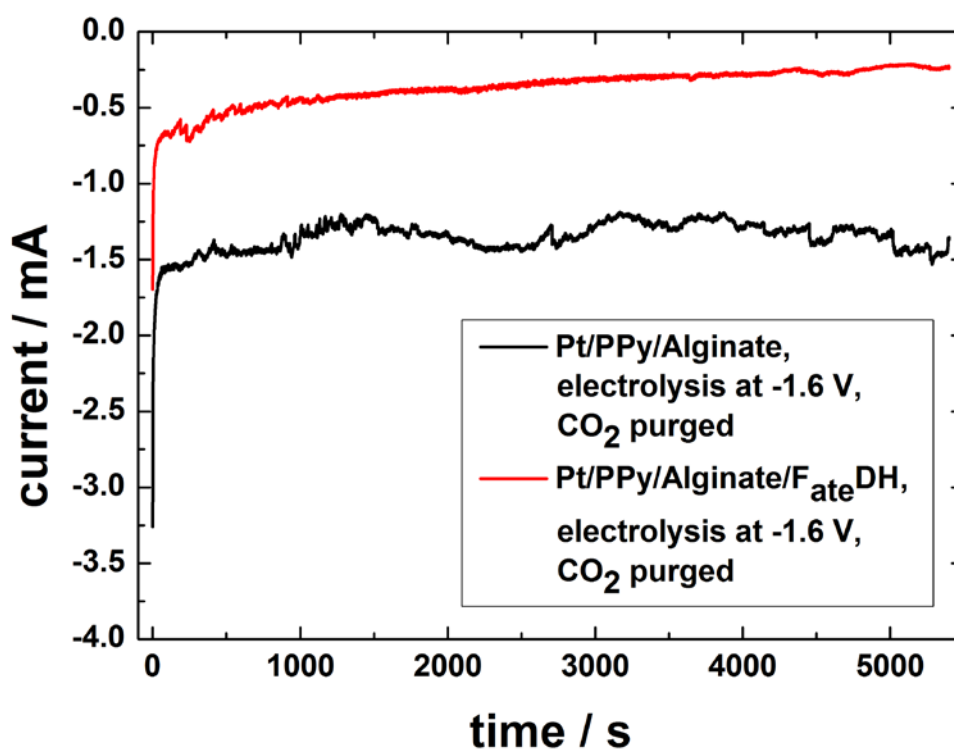


Figure 29: Current time curves recorded during electrolysis at -1.6 V with a Pt/PPy/Alginate/ $F_{ate}DH$ electrode and a blank Pt/PPy/Alginate electrode without enzyme modification. With enzyme modified electrode, less current is flowing, which proposes that the side reaction of water splitting is suppressed in case of the enzyme-modified system.

In Figure 30 the ion chromatogram of the electrolyte solution after electrolysis with a Pt/PPy/Alginate/ $F_{ate}DH$ electrode is shown. Electrolysis was conducted at

-1.4 V and -1.6 V. From samples after electrolysis at -1.4 V, no formate could be detected. Only during the electrolysis at -1.6 V formate was produced. 0.44 mmol/L formate, corresponding to a faradaic efficiency of 85%, were detected after electrolysis at -1.6 V for 1.5 h. Formate eluted at 6.3 min and was identified by comparison with an external standard calibration with formate standards of different concentrations. After electrolysis with a Pt/PPy/Alginate electrode without enzyme modification carried out for reference, no significant amounts of formate could be detected, which is shown in Figure 31. The peaks from 5.0 min to 5.9 min correspond to fluoride and acetate, which are impurities from the environment and from laboratory equipment used to inject the samples into the ion chromatograph.

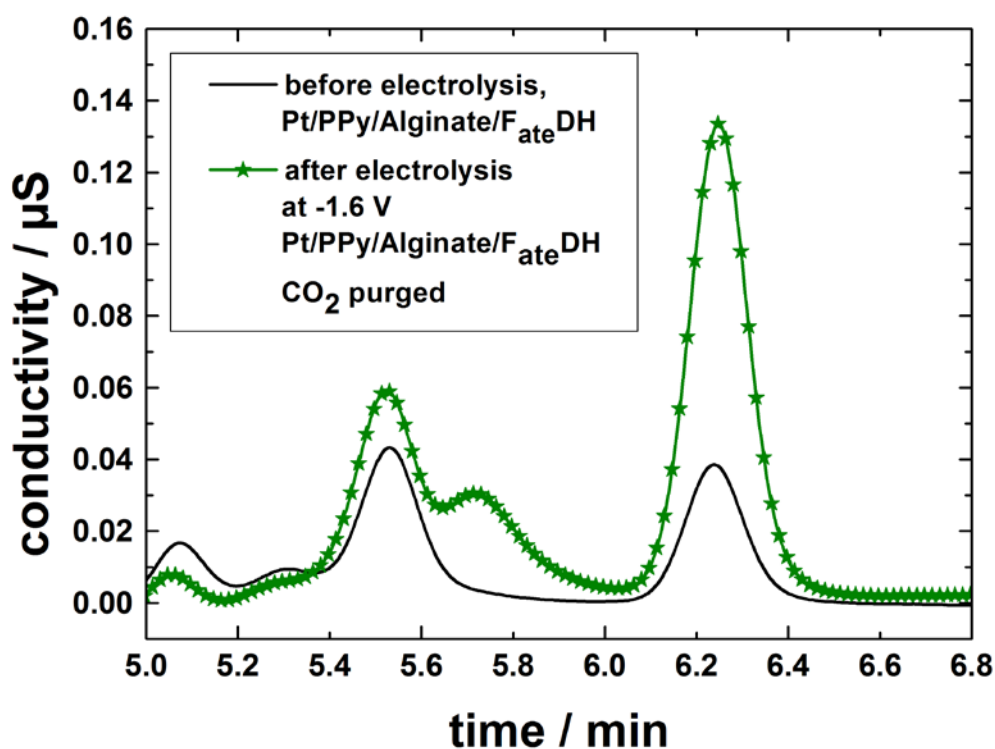


Figure 30: Ion chromatogram of the electrolyte solution after electrolysis at -1.6 V for 1.5 h showing a formate peak at 6.3 min. The peaks from 5.0 min to 5.9 min correspond to fluoride and acetate, which are contaminants from the environment and from laboratory equipment.

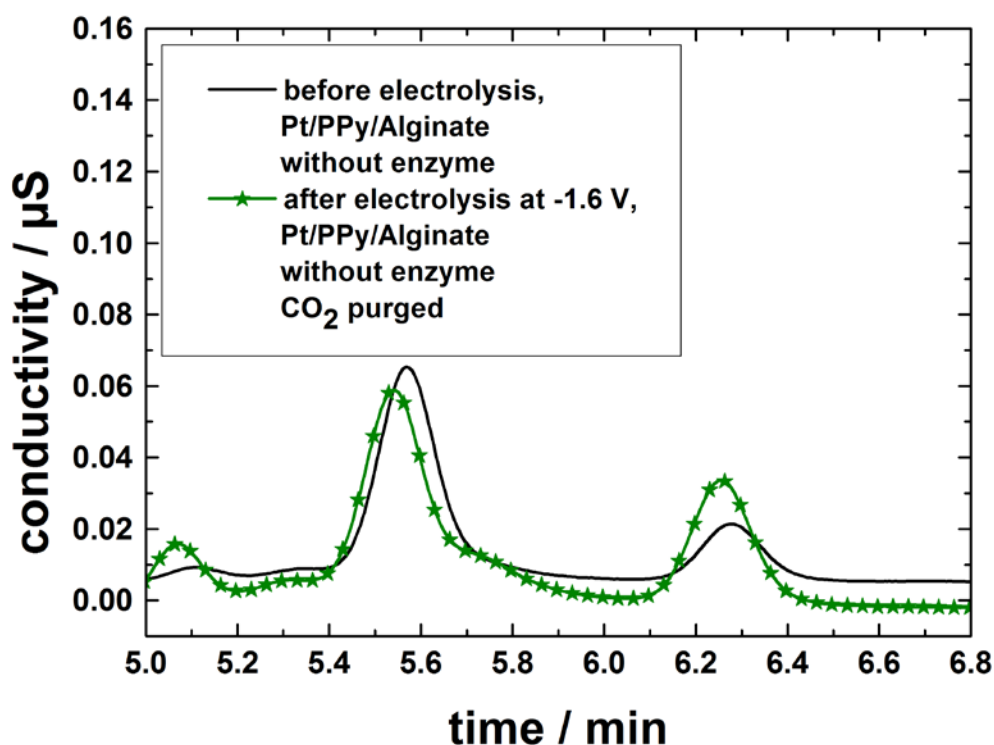


Figure 31: Ion chromatogram of the electrolyte solution after electrolysis at -1.6 V with a blank Pt/PPy/Alginate electrode without enzyme modification carried out for reference. No significant amounts of formate were detected.

3.2.3. Faradaic efficiency of formate production at Pt/PPy/Alginate/ $F_{ate}DH$ electrodes

The faradaic efficiency was calculated analogously to 3.1.3. The moles of electrons were divided by 2, because formate production out of CO_2 is a 2 electron process.



Duration of Electrolysis: 1.5 h = 5400 s

Mean electric current flow during electrolysis: $- 3.66 \cdot 10^{-4}$ A

$$Q = I \cdot t = 3.66 \cdot 10^{-4} \text{ A} \cdot 5400 \text{ s} = 1.98 \text{ A s} = 1.98 \text{ C}$$

$$X = \frac{Q}{F} = \frac{1.98 \text{ C}}{96485 \frac{\text{C}}{\text{mol}}} = 2.05 \cdot 10^{-5} \text{ moles of electrons}$$

$$n_{th} = \frac{\text{moles of electrons}}{2e^-} = \frac{2.05 \cdot 10^{-5} \text{ mol } e^-}{2e^-} = 1.03 \cdot 10^{-5} \text{ moles}$$

$$\eta_F = \frac{n_{\text{HCOO}^-}}{n_{\text{th}}} = \frac{8.80 \cdot 10^{-6} \text{ mol}}{1.03 \cdot 10^{-5} \text{ mol}} = 85 \%$$

3.2.4. Stability of Pt/PPy/Alginate/F_{ate}DH electrodes

The stability of platinum electrodes coated with a polypyrrole film and a F_{ate}DH-modified alginate layer is rather low. During electrolysis sometimes cracks on the electrode surface were formed, which is depicted in Figure 32. The alginate gel does not stick very tightly to the polypyrrole surface which results in instability in opposition to the carbonfelt electrodes, where a large sponge-like surface is provided for adherence of the alginate gel.



Figure 32: Pt electrode modified with polypyrrole film and an alginate layer containing F_{ate}DH with crack in the alginate layer formed during electrolysis.

3.3. Pt/PPy/F_{ate}DH Electrodes

3.3.1. Characterization of Pt/PPy/F_{ate}DH electrodes

CVs of platinum electrodes coated with a polypyrrole film containing F_{ate}DH (Pt/PPy/F_{ate}DH) were recorded at negative sweeping potentials of -1.4 V and -1.8 V in N₂ and CO₂ purged systems to figure out the best potential for formate production.

Figure 33 and Figure 34 show the CVs of a Pt/PPy/F_{ate}DH electrode in N₂ (black curve) and CO₂ (red curve) saturated systems at negative sweeping potentials of -1.4 V and -1.8 V. The increase in current for the reduction of CO₂ is about 0.05 mA at -1.4 V and about 0.07 mA at -1.8 V, starting in both cases at about -1.0 V.

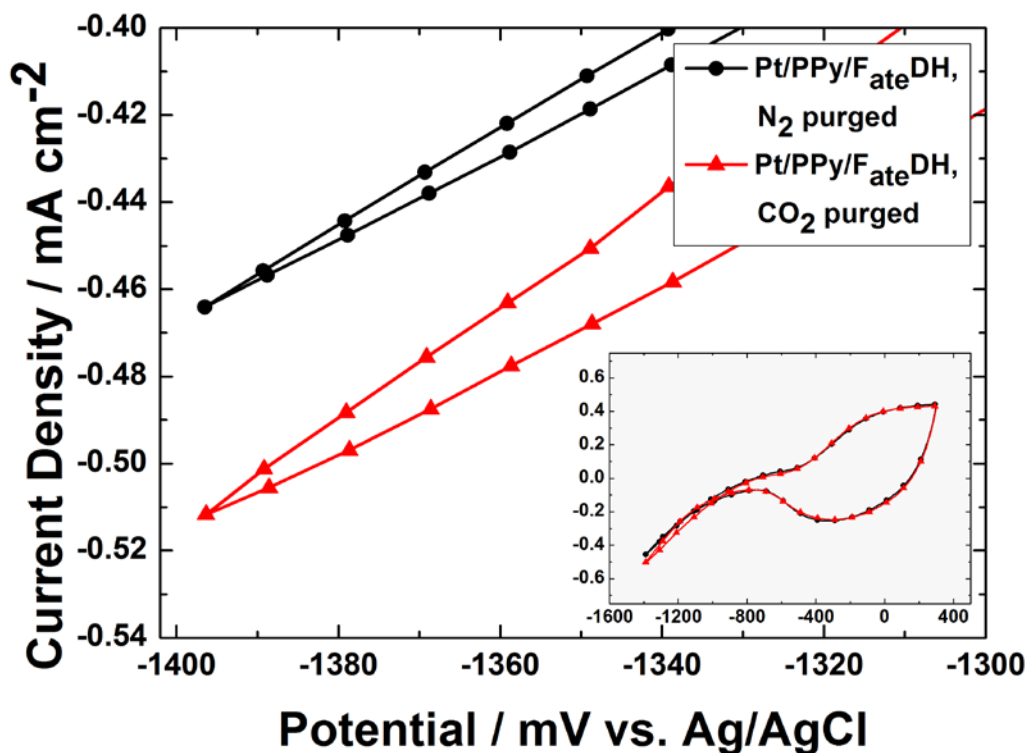


Figure 33: CVs of a Pt/PPy/F_{ate}DH electrode at a negative sweeping potential of -1.4 V vs. Ag/AgCl. Comparison of CVs of the N₂ purged system (black curve) to the CVs recorded in the CO₂ purged system (red curve) with a distinct increase in reductive current for the CO₂ purged system starting at about -1.0 V.

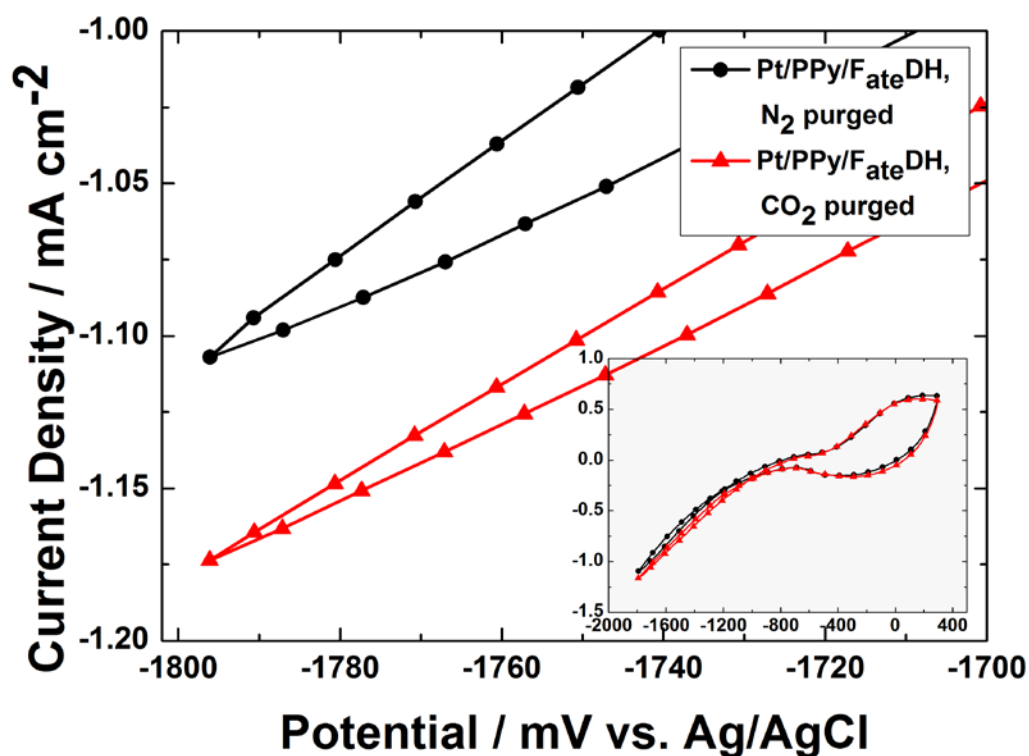


Figure 34: CVs of a Pt/PPy/F_{ate}DH electrode at a negative sweeping potential of -1.8 V vs. Ag/AgCl. Comparison of CVs recorded in the N₂ purged system and in the CO₂ purged system with distinct increase in reductive current for the CO₂ purged system starting at about -1.0 V.

The CV of a Pt/PPy electrode without enzyme modification in a CO₂ saturated electrolyte solution does not show a higher reductive current flow than when saturated with N₂, which is apparent in Figure 35.

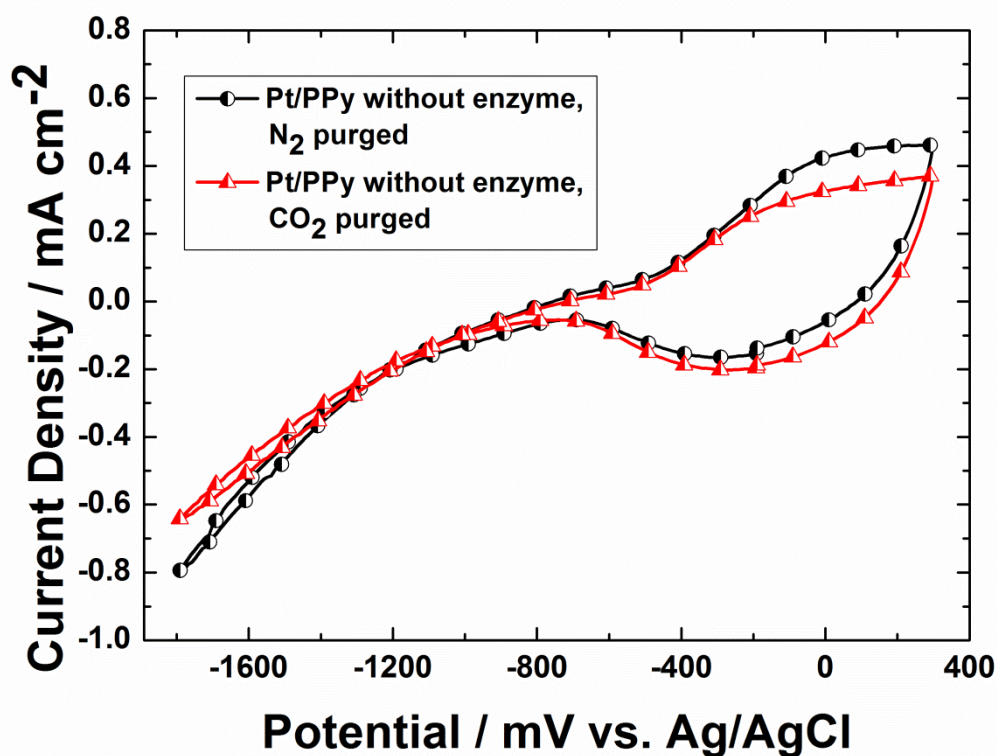


Figure 35: CVs of a Platinum electrode modified with polypyrrole film without enzyme modification. Comparison of CVs recorded in N_2 (black curve) and CO_2 (red curve) purged systems. No increase in reductive current for the CO_2 purged system is observed in relation to the N_2 purged system.

The comparison of CVs of Pt/PPy/ $F_{ate}DH$ electrodes to Pt/PPy electrodes without enzyme modification reveals a much higher reductive current in a CO_2 purged system with the enzyme modified electrode in relation to the bare Pt/PPy electrode (See Figure 36).

Due to this large effect for CO_2 reduction for the enzyme modified electrode at a potential of -1.8 V, this potential was applied for electrolysis and gave the best results of formate yield, whereas after electrolysis at lower potentials, no formate could be detected.

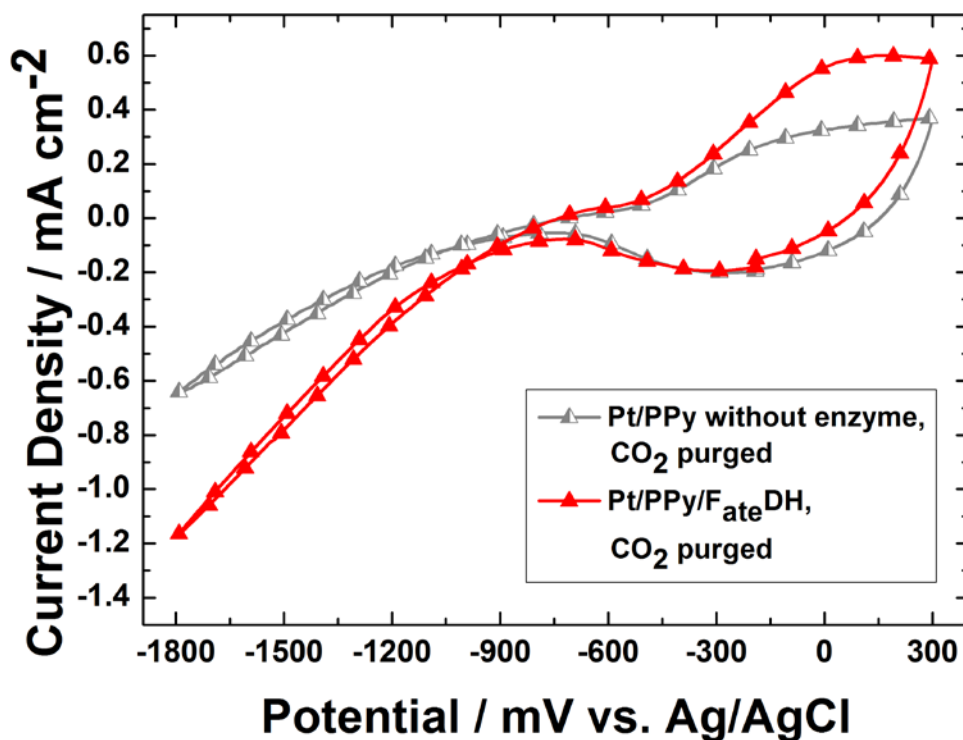


Figure 36: Comparison of the CVs of a platinum electrode modified with a polypyrrole film without enzyme (grey curve) and a platinum electrode modified with polypyrrole containing F_{ate}DH (red curve). The CO₂ purged system with F_{ate}DH modification shows much higher reductive current at -1.8 V than the CO₂ purged system without enzyme modification.

After electrolysis at -1.8 V, 5.4 mmol/L formate were produced. After electrolysis carried out at -1.4 V no formate could be detected. Furthermore, electrolysis with Pt/PPy electrodes without enzyme modification at -1.8 V conducted for reference did not yield formate.

In theory, the potential for CO₂ reduction to formate is at -0.61 V vs. NHE, which is about -0.8 V vs. Ag/AgCl. However, potentials of at least -1.8 V have to be applied during electrolysis to yield detectable amounts of formate. We assume that this high overpotential at Pt/PPy/F_{ate}DH electrodes results from the fact that the diffusion of substrate (CO₂) to the active centers of the enzymes is limited as the enzymes are incorporated into the pyrrole polymer and the active centers are not always available on the surface of the polymer electrode.

3.3.2. Electrolysis with Pt/PPy/F_{ate}DH electrodes

Figure 37 shows the current-time curves recorded during electrolysis at -1.8 V with a Pt/PPy/F_{ate}DH and a Pt/PPy electrode without enzyme modification. These curves, however do not allow conclusions about the assumption of suppression of side reactions by enzymes, as the system was not stable during electrolysis. At some places of the electrode, delamination of the polypyrrole film occurred, which revealed the blank platinum surface, allowing water splitting to occur more dominantly.

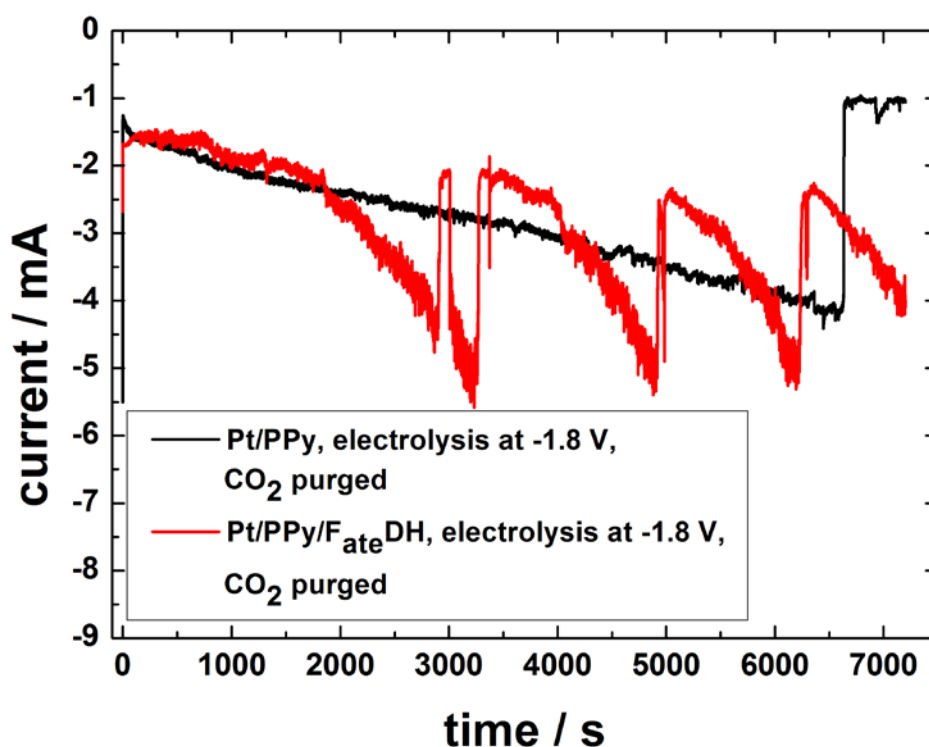


Figure 37: Current-time curves recorded during electrolysis at -1.8 V with a Pt/PPy/F_{ate}DH electrode and a blank Pt/PPy electrode without enzyme modification. The peaks in the current are due to instability and delamination of the polypyrrole film during electrolysis.

Figure 38 shows the ion chromatogram of the electrolyte solution after electrolysis with a Pt/PPy/F_{ate}DH electrode at -1.8 V for 2 h. The peak at 6.2 min was identified as formate by external standard calibration. 5.4 mmol/L formate were produced, which corresponds to a faradaic efficiency of about 40%. The peak at 5.4 min corresponds to acetate which is an impurity from the plastic in the syringes, which were used to inject the samples into the ion chromatograph. For electrolysis with a Pt/PPy electrode without enzyme modification at -1.8 V

conducted for reference, a little amount of formate compared to the enzyme modified system could be detected, which suggests a catalytic effect of polypyrrole for CO₂ reduction (See Figure 39).

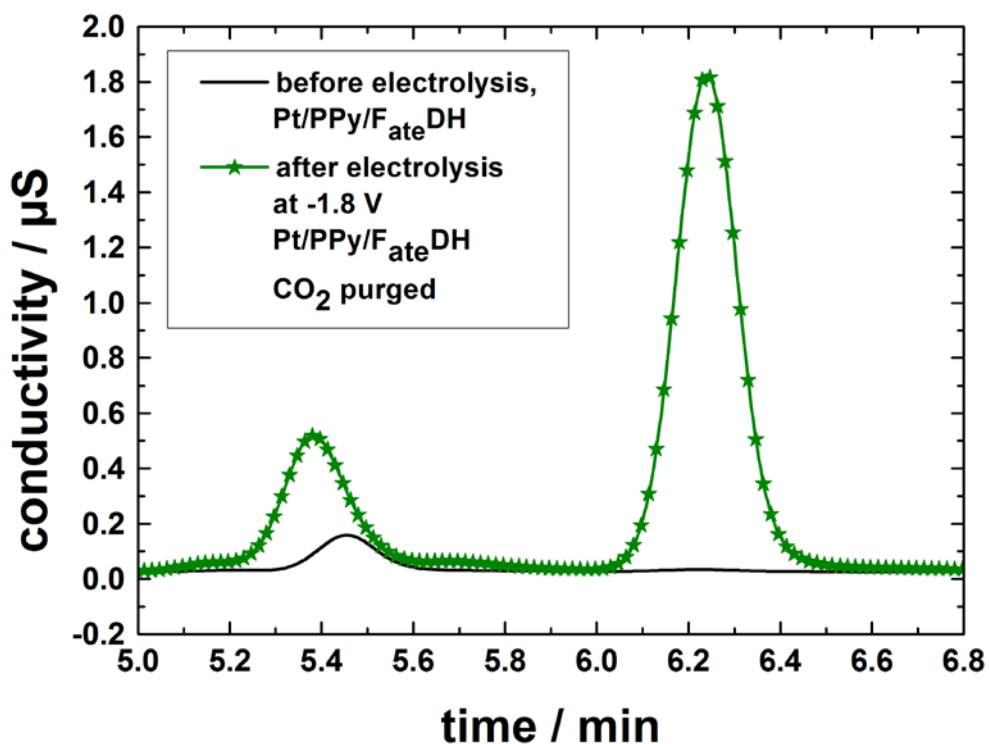


Figure 38: Ion Chromatogram of the electrolyte solution after 2 h electrolysis at -1.8 V of a Pt/PPy/F_{ate}DH electrode. A formate peak can be seen at 6.3 min. The peak at 5.4 min corresponds to acetate, which is a contaminant from the plastic in the syringes used to inject the samples.

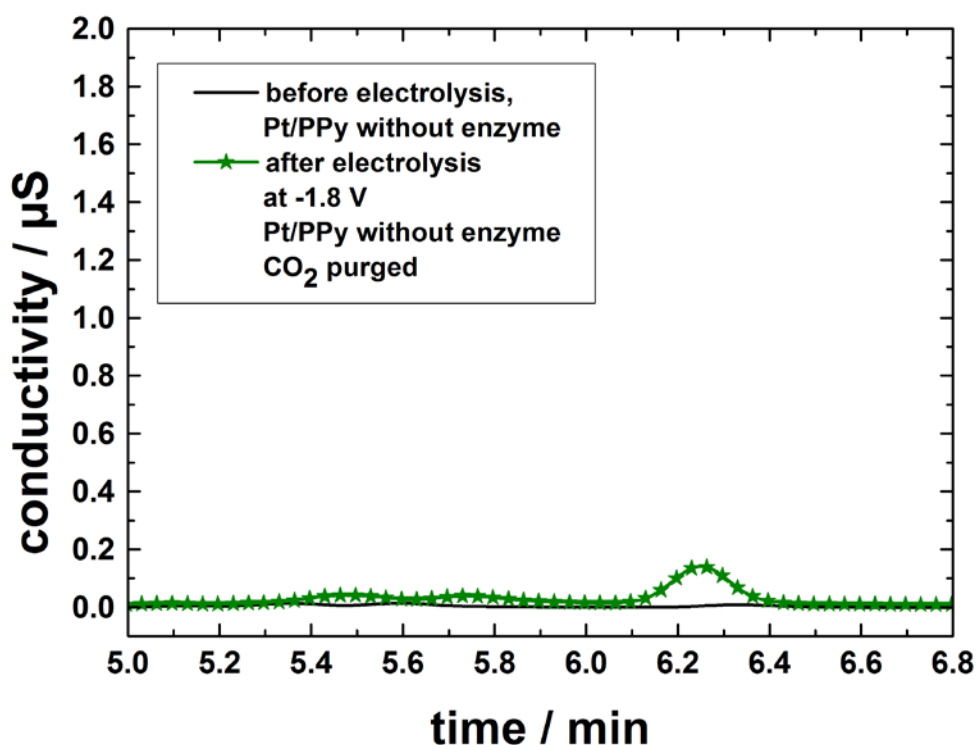


Figure 39: Ion chromatogram of the electrolyte solution after electrolysis at -1.8 V with a blank Pt/PPy electrode without enzyme modification carried out for reference. There is a small formate peak at 6.3 min, suggesting a catalytic effect of polypyrrole for CO₂ reduction.

3.3.3. Faradaic efficiency of formate production at Pt/PPy/F_{ate}DH electrodes

The faradaic efficiency of formate production is calculated analogous to 3.2.3.

Duration of electrolysis: 2 h = 7200 s

Mean electric current flow during electrolysis: $- 2.89 \cdot 10^{-3}$ A

$$Q = I \cdot t = 2.89 \cdot 10^{-3} \text{ A} \cdot 7200 \text{ s} = 20.83 \text{ A s} = 20.83 \text{ C}$$

$$X = \frac{Q}{F} = \frac{20.83 \text{ C}}{96485 \frac{\text{C}}{\text{mol}}} = 2.16 \cdot 10^{-4} \text{ moles of electrons}$$

$$n_{\text{th}} = \frac{\text{moles of electrons}}{2 e^-} = \frac{2.16 \cdot 10^{-4} \text{ mole}^-}{2 e^-} = 1.08 \cdot 10^{-4} \text{ moles}$$

$$\eta_{\text{F}} = \frac{n_{\text{HCOO}^-}}{n_{\text{th}}} = \frac{4.05 \cdot 10^{-5} \text{ mol}}{1.08 \cdot 10^{-4} \text{ mol}} = 38 \%$$

3.3.4. Stability of Pt/PPy/ $F_{ate}DH$ electrodes

The platinum electrodes coated with a polypyrrole film containing $F_{ate}DH$ were not stable during electrolysis. The polypyrrole film was peeled away at some places on the electrode, presumably due to hydrogen evolution, which can be seen in Figure 40.



Figure 40: Pt/PPy/ $F_{ate}DH$ electrode after electrolysis. At some places the PPy film was peeled away.

3.3.5. Microscopic characterization of the Pt/PPy/ $F_{ate}DH$ electrodes

Pt/PPy electrodes modified with $F_{ate}DH$ and without enzyme modification were examined under a microscope. Furthermore, the surface of the blank platinum electrode was investigated.

Figure 41 depicts a Pt/PPy/ $F_{ate}DH$ electrode before and after electrolysis at 1000x magnification. Compared to the Pt/PPy/ $F_{ate}DH$ electrode surface before electrolysis it is apparent that there is a place where the polypyrrole film was peeled off during electrolysis. Nonetheless, on the places where polypyrrole is still there after electrolysis, the polymer film looks unchanged.

Figure 42 displays the Pt/PPy/F_{ate}DH electrode at 4000x magnification, which offers a more detailed look on the surface of the polymer film.

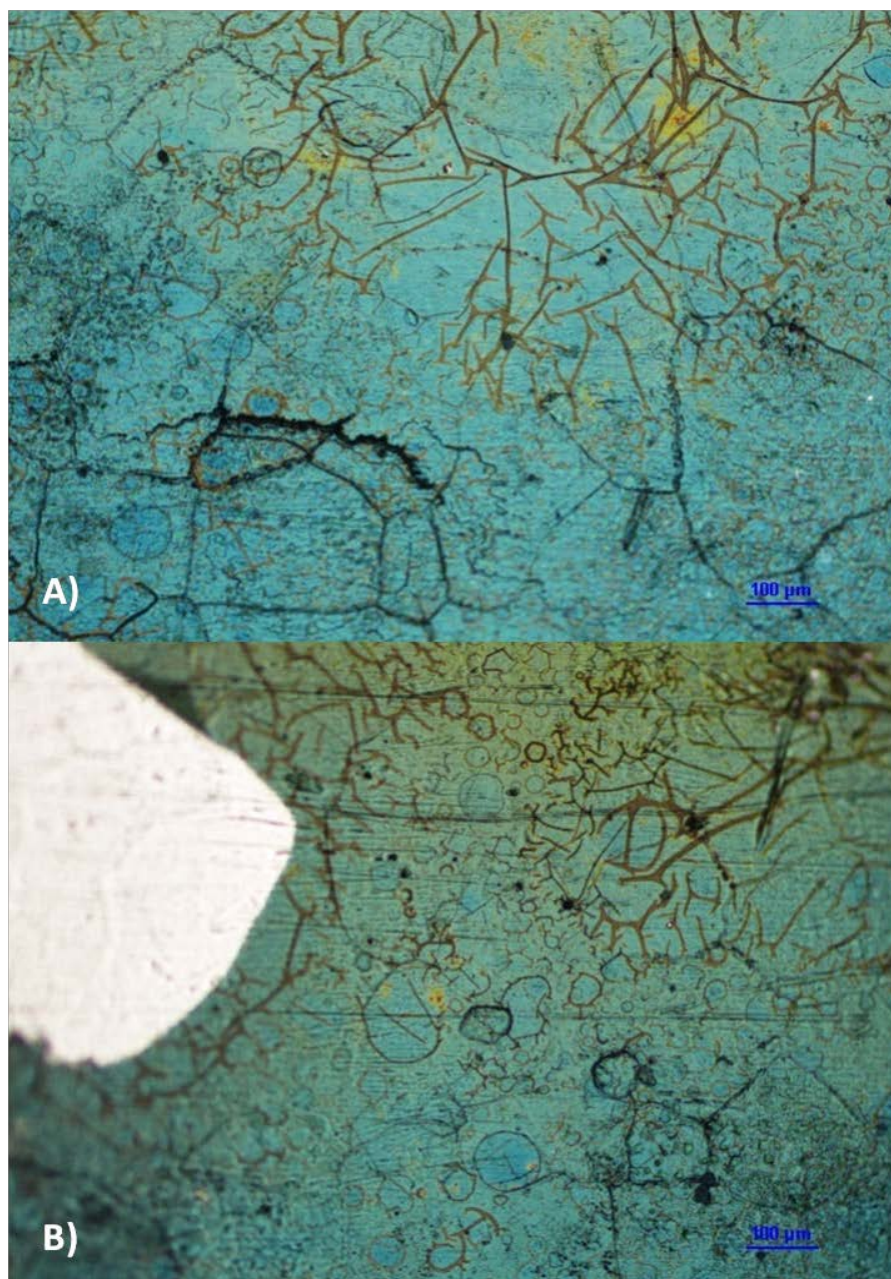


Figure 41: Pt/PPy/F_{ate}DH electrode at 1000x magnification. A) electrode surface before electrolysis. B) electrode surface after electrolysis. It is obvious that the polypyrrole film was peeled away at one place during electrolysis.

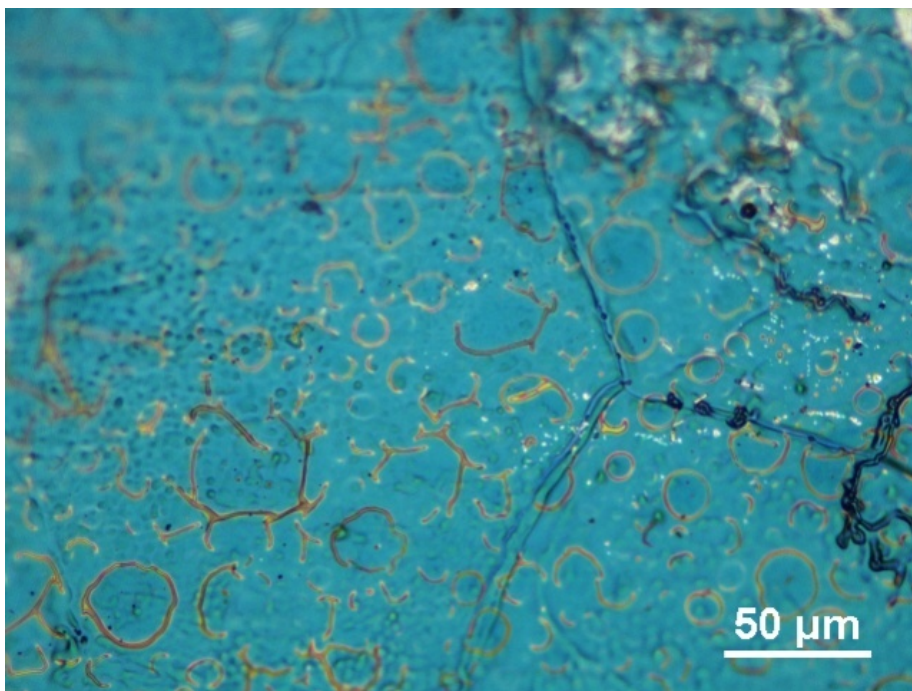


Figure 42: Pt/PPy/F_{ate}DH electrode; electrode surface before electrolysis at 4000x magnification.

In Figure 43 the surface of a Pt/PPy electrode without enzyme modification after electrolysis is depicted. It is obvious that the polypyrrole film was peeled away during electrolysis.

In contrast to the enzyme modified Pt/PPy/F_{ate}DH electrode depicted in Figure 41, it can be seen that the holes in the polypyrrole film are bigger and in a higher quantity at the surface of the Pt/PPy electrode without enzyme modification.

Figure 44 shows the Pt/PPy electrode at 4000x magnification, which again enables a detailed look at the surface composition of the polypyrrole film. The blue part depicts the polypyrrole film, the red part shows a region where a double layer of polypyrrole formed as a result of peeling off of the polymer film.

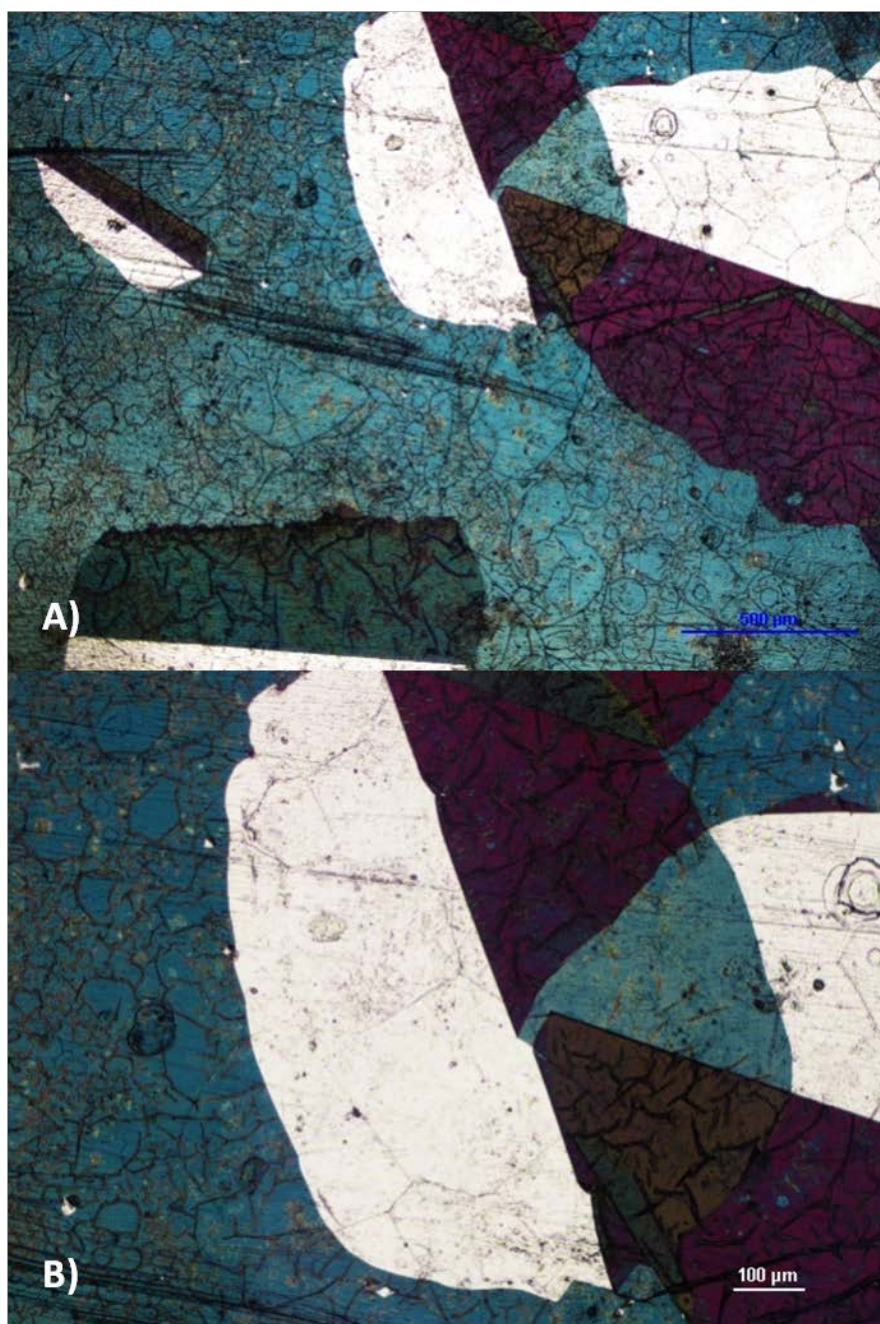


Figure 43: Pt/PPy electrode without enzyme modification after electrolysis at 500x magnification (A) and 1000x magnification (B). The polypyrrole film was peeled off during electrolysis at some points of the electrode.

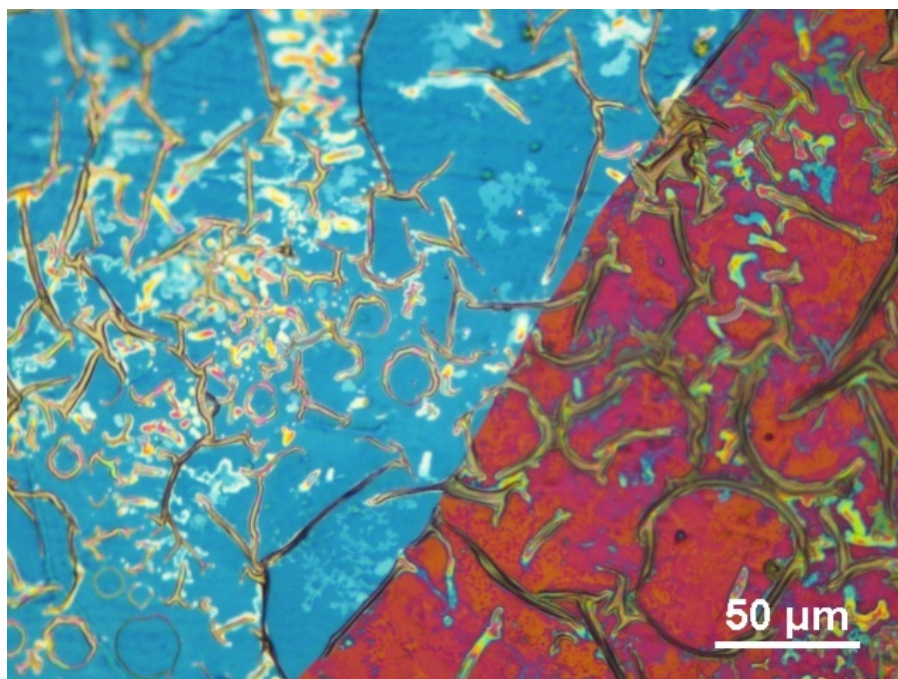


Figure 44: Pt/PPy electrode without enzyme modification after electrolysis at 4000x magnification. The blue part depicts the polypyrrole film, the red part shows a region where a double layer of polypyrrole formed as a result of peeling off of the polymer film.

The surface of the cleaned platinum electrode is depicted in Figure 45. The surface of the electrode shows scratches and irregularities which does not allow a perfect adsorption of enzymes. Thus, irregular adsorption and subsequent electropolymerisation of pyrrole onto the electrode occur which can affect the function of the electrodes.

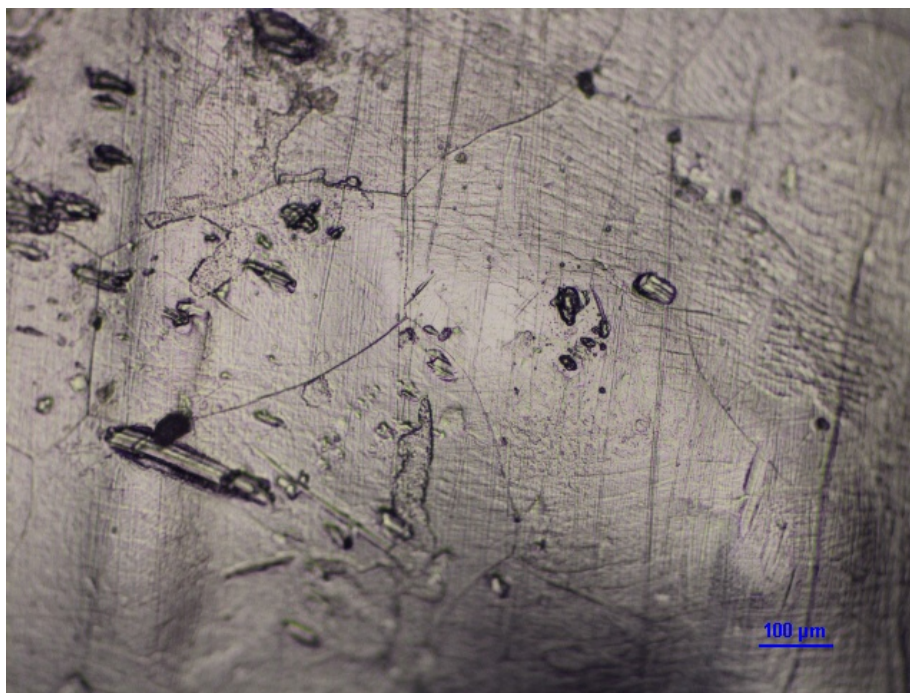


Figure 45: The blank platinum electrode at 1000x magnification shows scratches and irregularities. Therefore irregular adsorption and subsequent electropolymerisation of pyrrole onto the electrode surface occur. This can affect the function of the electrode.

3.4. Physical Adsorption of $F_{ate}DH$ on Graphite Rods

3.4.1. Characterization of Graphite/ $F_{ate}DH$ electrodes

CVs of graphite electrodes modified with adsorbed $F_{ate}DH$ (graphite/ $F_{ate}DH$) were recorded at different negative sweeping potentials of -1.0 V and -1.4 V vs. Ag/AgCl. Higher negative potentials were not investigated because the characterization of blank graphite electrodes to the region above -1.4 V showed excessive hydrogen evolution, which is in concurrence to CO_2 reduction, limiting the faradaic efficiency of formate production.

Figure 46 shows the CVs of a graphite/ $F_{ate}DH$ electrode at a negative sweeping potential of -1.0 V. The CV of the graphite/ $F_{ate}DH$ electrode exhibits a small increase in reductive current of for the CO_2 purged system relative to the N_2 purged system of about 0.04 mA. The increase in current for CO_2 reduction related to the N_2 purged system starts at about -0.5 V

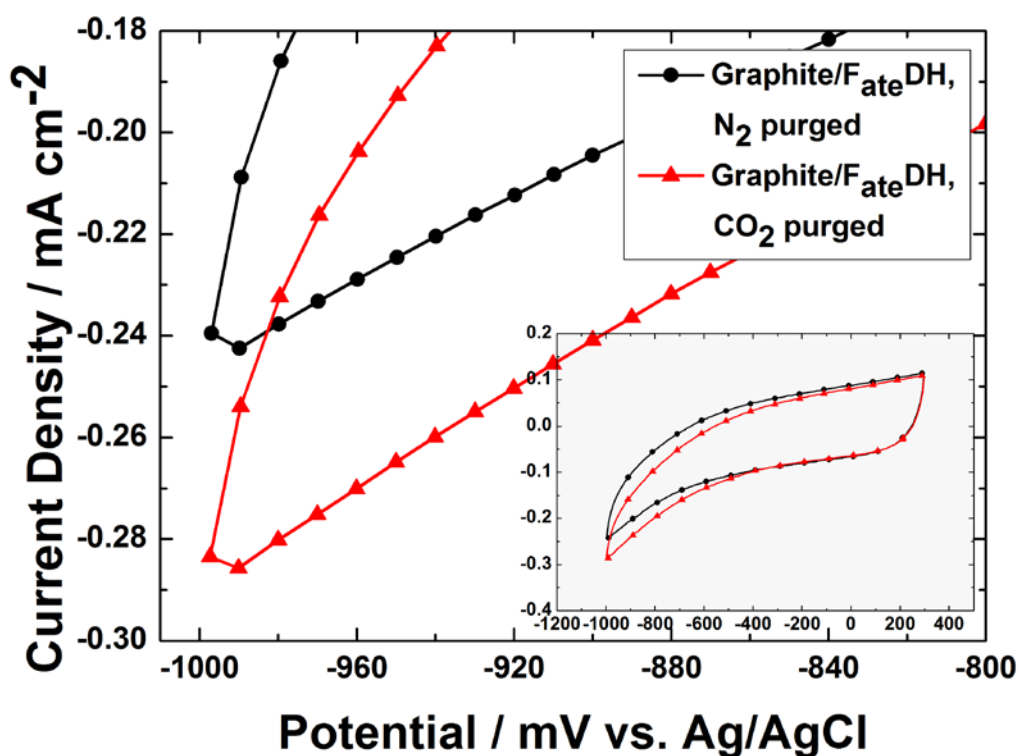


Figure 46: Comparison of CVs of a Graphite/ $F_{ate}DH$ electrode recorded in the N_2 purged system (black curve) and the CO_2 purged system (red curve) at a negative sweeping potential of -1.0 V vs. Ag/AgCl. The CO_2 purged system shows an increase in reductive current in relation to the N_2 purged system starting at about -0.5 V.

Figure 47 displays the CVs of a graphite/ $F_{ate}DH$ electrode at a negative sweeping potential of -1.4 V in N_2 and CO_2 purged systems. The CV of the graphite/ $F_{ate}DH$ electrode shows only about 0.15 mA increase in reductive current for the CO_2 purged system in comparison to the N_2 purged system at -1.4 V.

The current for CO_2 reduction in relation to the N_2 purged system starts to increase at about -0.5 V.

A point which has to be considered is that the CV of the blank graphite electrode also shows a high increase in reductive current of about 0.4 mA for the CO_2 purged system in comparison to the N_2 purged system (See Figure 48). This indicates that the enzymes in the Graphite/ $F_{ate}DH$ electrode are not reducing the CO_2 , as even the blank graphite electrode shows an increase in reductive current when the system is saturated with CO_2 .

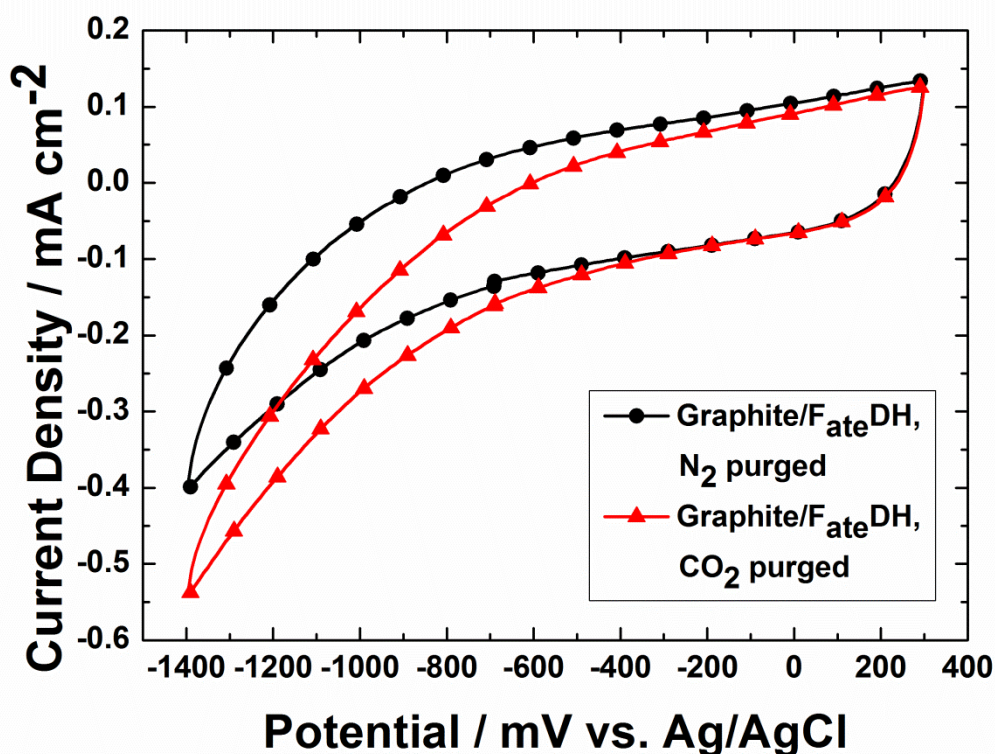


Figure 47: Comparison of CVs of a Graphite/F_{ate}DH electrode recorded in the N₂ purged system (black curve) and the CO₂ purged system (red curve) at a negative sweeping potential of -1.4 V vs. Ag/AgCl with a distinct increase in reductive current for the CO₂ purged system starting at about -0.5 V.

After electrolysis with graphite/F_{ate}DH electrodes at -1.0 V and -1.4 V no formate could be detected.

Figure 48 shows the CVs of a blank graphite electrode measured in N₂ and CO₂ purged systems at a negative sweeping potential of -1.4 V. The characterization of this graphite electrode shows also an increase in reductive current for the CV recorded in a CO₂ saturated system in relation to the CV recorded in a N₂ purged system. Thus, most likely graphite also is reducing CO₂ to higher energy molecules. However, this study is only focused on formate production and other possible products were not investigated.

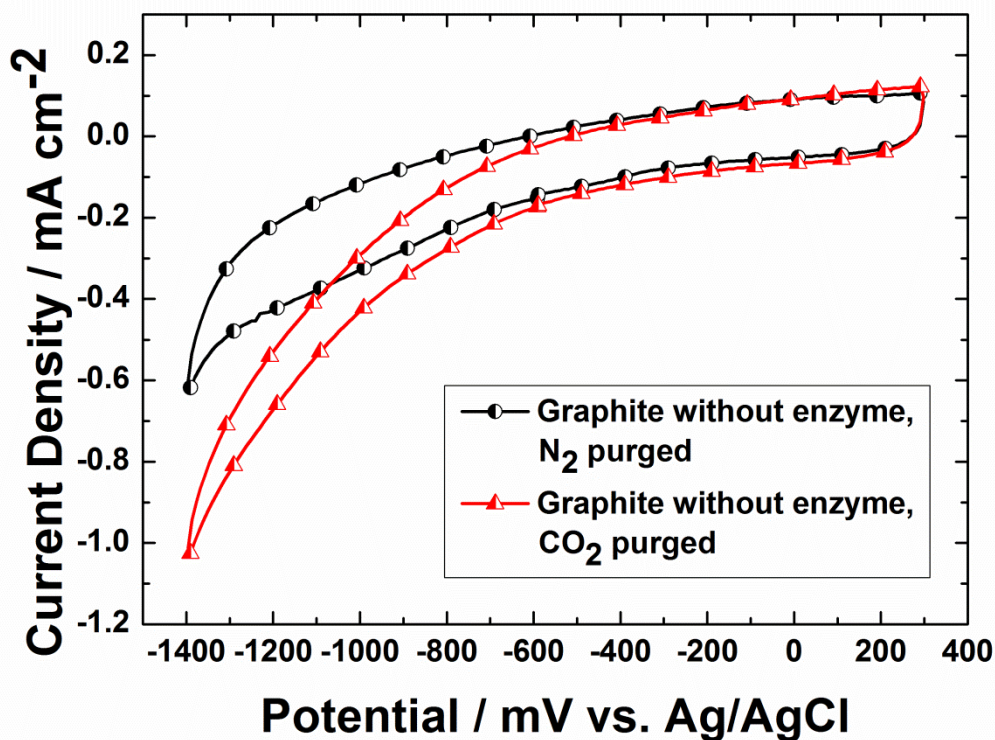


Figure 48: Comparison of CVs of a blank graphite electrode recorded in N_2 purged (black curve) and CO_2 purged (red curve) systems. An increase in reductive current for the CO_2 purged system in relation to the N_2 purged system was observed.

After electrolysis with graphite/ $F_{ate}DH$ electrodes at -1.0 V and -1.4 V, no formate could be detected.

3.4.2. Electrolysis with a Graphite/ $F_{ate}DH$ electrode

Figure 49 depicts the current-time curves recorded during electrolysis at -1.4 V with a Graphite/ $F_{ate}DH$ electrode and a blank graphite electrode without enzyme modification. It can again be seen, that during electrolysis with the enzyme modified electrode, less current is flowing than in the case of the blank graphite electrode. This suggests again, that the enzymes suppress side reactions and only the formation of one specific product is favored.

Nonetheless, no significant amounts of formate could be detected after electrolysis at -1.4 V with enzyme modified graphite electrodes and with blank graphite electrodes.

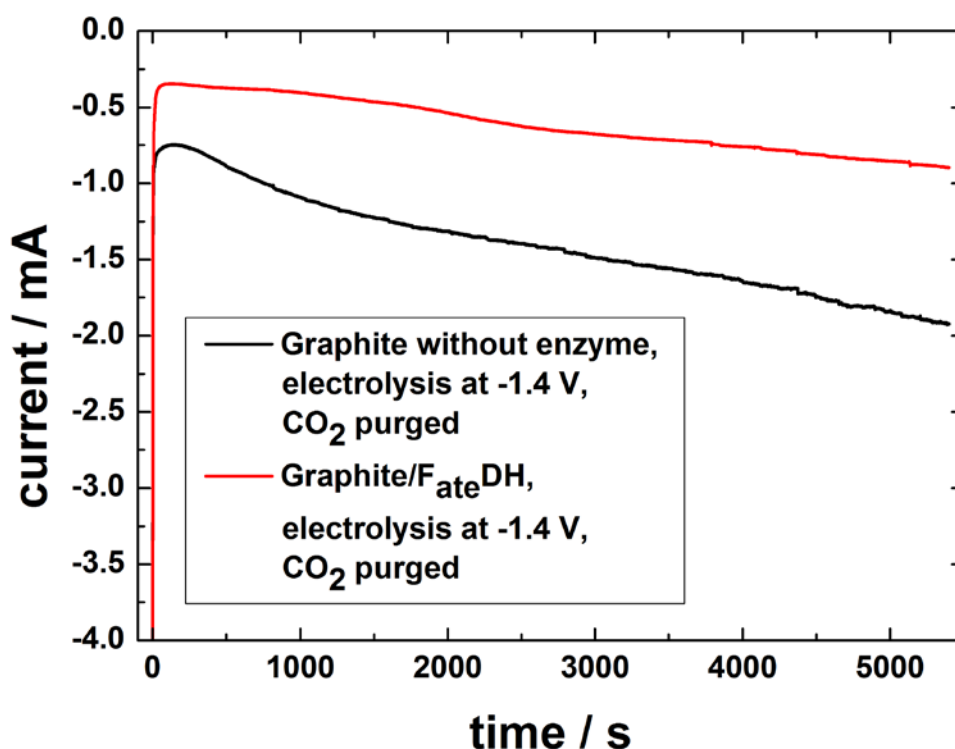


Figure 49: Current-time curves recorded during electrolysis with a Graphite/F_{ate}DH electrode and with a blank graphite electrode. During electrolysis with the enzyme modified electrode less current is flowing than in case of the blank graphite electrode, suggesting the suppression of side reactions in case of the enzyme modified electrode.

After electrolysis at -1.4 V with graphite electrodes modified with F_{ate}DH, no significant amounts of formate could be detected, as shown in the ion chromatograms recorded after electrolysis with a Graphite/F_{ate}DH electrode and a blank graphite electrode without enzyme modification (See Figure 50 and Figure 51). The reason might be that the enzyme was only physically adsorbed onto the graphite surface and no further stabilization was done. We assume that due to the electric current during electrolysis, the weak Van der Waals interactions broke and the three dimensional structure of the enzyme changed so that the activity was lost.

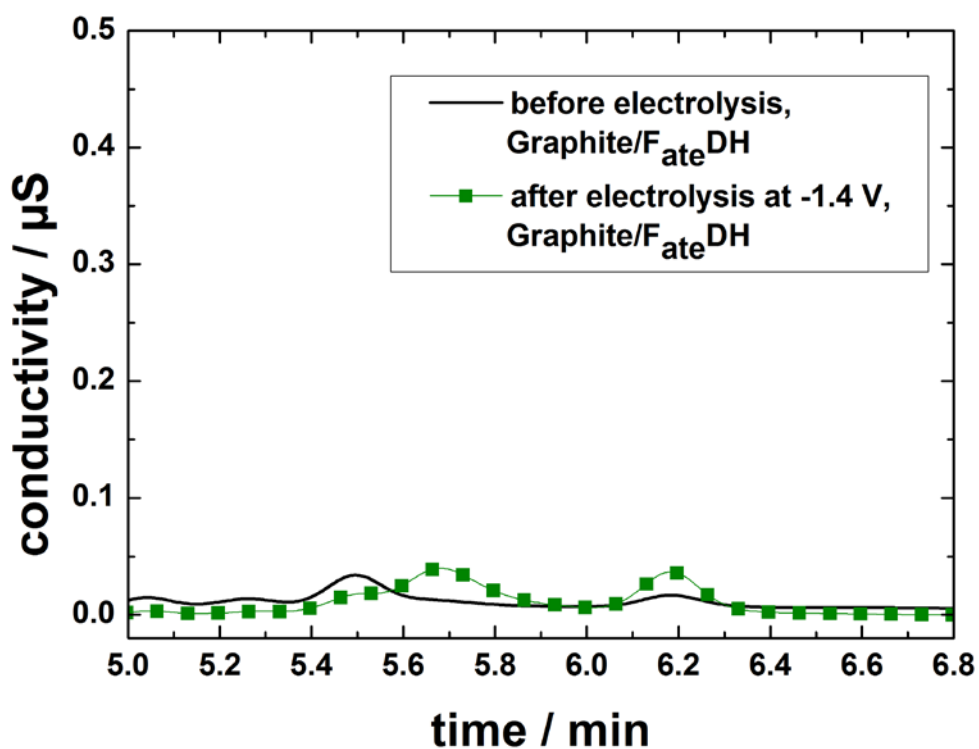


Figure 50: Ion chromatogram of the electrolyte solution after electrolysis at -1.4 V with a Graphite/ $\text{F}_{\text{ate}}\text{DH}$ electrode. No significant amounts of formate were detected.

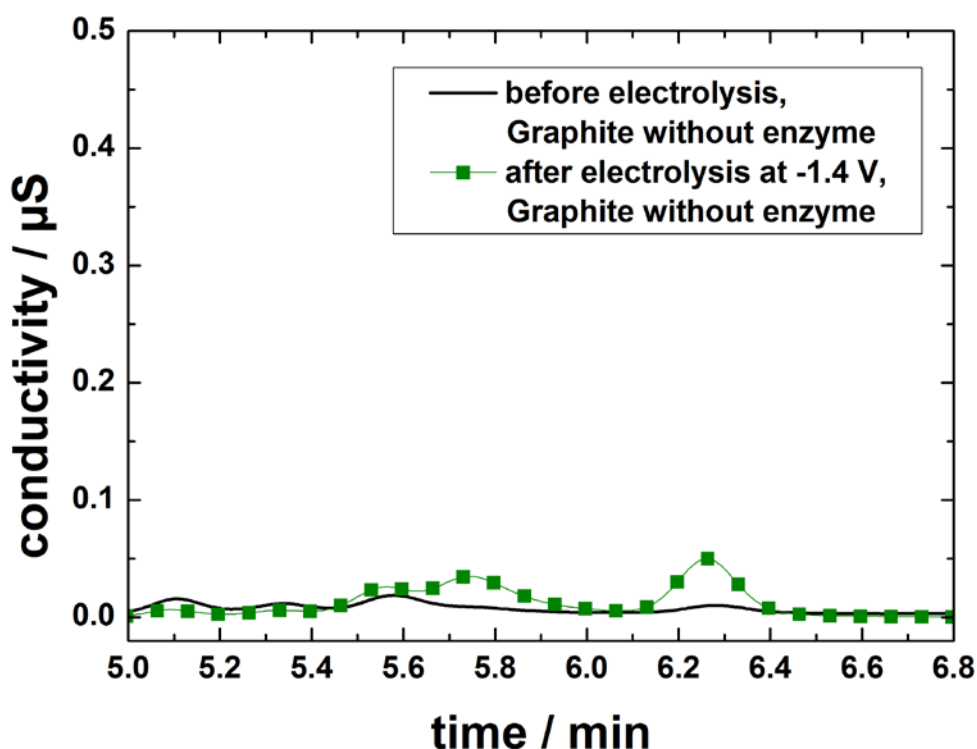


Figure 51: Ion chromatogram of the electrolyte solution after electrolysis at -1.4 V with a blank graphite electrode without enzyme modification carried out for reference. No significant amounts of formate were detected.

4. Conclusion

This work shows the direct electrochemical reduction of CO₂ to formate and methanol catalyzed by dehydrogenases, enabling an attractive way to synthesize higher energy molecules from CO₂. Substitution of the expensive, sacrificial co-enzyme NADH as well as mild reaction conditions such as moderate temperatures and low pressures help to reduce the process costs significantly compared to industrial methods used today where high pressures and temperatures are required. Furthermore, immobilization of the enzymes on electrodes enables their re-usage and a sustainable and biodegradable CO₂ reduction process is provided.

The most efficient way of CO₂ reduction was reached with carbonfelt electrodes modified with an alginate-enzyme layer as reported by S. Schlager et al. [35]. Carbonfelt provides a big surface area which increased the reaction efficiency and improved the adhesion of the alginate layer to the electrode. Moreover, these electrodes showed the highest stability.

With Pt/PPy/Alginate/F_{ate}DH electrodes and Pt/PPy/F_{ate}DH electrodes, formate production could be achieved with faradaic efficiencies of about 85% and 40%. However, the stability of the systems was not very promising. In the alginate layer, cracks were sometimes formed during electrolysis and in the case of Pt/PPy/F_{ate}DH electrodes, at some points of the electrodes, the polypyrrole film was peeled off.

Moreover, it was realized, that cyclic voltammetry might not be a convincing method to characterize these enzyme modified electrodes, as even though in most CVs the effect of CO₂ reduction was not very big, high faradaic efficiencies could be achieved. Further, the assumption has been made, that the enzymes are suppressing unwanted side reactions like water splitting and thus using the current more efficiently, which has been suggested by the current-time curves recorded during electrolysis.

Even though the theoretical potentials for CO₂ reduction to formate and methanol are -0.61 V vs. NHE (-0.8 V vs. Ag/AgCl) and -0.38 V vs. NHE (-0,6 V vs. Ag/AgCl), for all systems, significant overpotentials of 0.6 V to 1.0 V had to be considered during electrolysis. Presumably, this is because of the low conductivity of the alginate layer and diffusion limitations of CO₂ to the enzymes due to the hindrance by the immobilization matrices. Higher overpotentials applied during electrolysis result in a lower faradaic efficiency because water splitting starts to get more dominantly.

As a result, the system has to be improved further concerning stability and faradaic efficiency of the reaction.

Nonetheless, enzyme immobilization on electrodes offers a sustainable and biodegradable way for CO₂ reduction and an independence of fossil fuels.

5. Acknowledgements

I wish to express my gratitude to o.Univ. Prof. Mag. Dr. DDr. h.c. Niyazi Serdar Sariciftci for giving me the opportunity to work at the Linz Institute for Physical Chemistry. Furthermore I want to thank DI Stefanie Schlager and DI Engelbert Portenkirchner for practical and content-related support.

6. References

- [1] Dr. Pieter Tans, NOAA/ESRL: Full Mauna Loa CO₂ record, (<http://www.esrl.noaa.gov/gmd/ccgg/trends/mlo.html> accessed: 13. Nov. 2013)
- [2] C. D. Keeling, R. B. Bacastow, A. E. Bainbridge, C. A. Ekdahl, P. R. Guenther, L.S. Waterman, *Tellus* **28** (1976) 538 - 551
- [3] J. R. Petit, I. Basile, A. Leruyet, D. Raynaud, C. Lorius, J. Jouzel, M. Stievenard, V.Y. Lipenkov, N.I. Barkov, B.B. Kudryashov, M. Davis, E. Saltzman, V. Kotlyakov, *Nature* **387**(1997) 359 - 360
- [4] J. R. Petit, J. Jouzel, D. Raynaud, N. I. Barkov, J. -M. Barnola, I. Basile, M. Benders, J. Chappellaz, M. Davis, G. Delayque, M. Delmotte, V. M. Kotlyakov, M. Legrand, V. Y. Lipenkov, C. Lorius, L. Pépin, C. Ritz, E. Saltzman, M. Stievenard, *Nature* **399** (1999) 429 - 436
- [5] J. M. Barnola, D. Raynaud, Y. S. Korotkevich, C. Lorius, *Nature* **329** (1987) 408 - 414
- [6] S. A. Rackley, Carbon Capture and Storage, (2010), Elsevier Inc.
- [7] R. L. Graham, F. B. Metting: Carbon Sequestration in terrestrial ecosystems, (<http://csite.ornl.gov/> accessed: 13. Nov. 2013)
- [8] G. A. Olah, *Angew. Chem. Int. Ed.* **44** (2005) 2636 – 2639
- [9] M. Aresta, Carbon Dioxide as a Chemical Feedstock, (2010), WILEY-VCH GmbH & Co. KG
- [10] M. Jitaru, *J. Chem. Technol. Metall.* **42** (2007) 333 - 344
- [11] J. Hawecker, J. Lehn, R. Ziessel, *J. Chem. Soc., Chem. Commun.* **6** (1984) 328 – 330
- [12] E. E. Benson, C. P. Kubiak, A. J. Sathrum, J. M. Smieja, *Chem. Soc. Rev.* **38** (2008) 89 - 99
- [13] E. Portenkirchner, K. Oppelt, D.A.M. Egbe, G. Knör, N. S. Sariciftci, *Nanomaterials and Energy* **2** (2013) 134 - 147
- [14] S. Cosnier, A. Deronzier, J. –C. Moutet, *J. Mol. Catal.* **45** (1988) 381- 391
- [15] E. B. Cole, P. S. Lakkaraju, D. M. Rampulla, A. J. Morris, E. Abelev, A. B. Bocarsly, *J. Am. Chem. Soc.* **132** (2010) 11539 - 11551
- [16] T. Mizuno, A. Naitoh, K. Ohta, *J. Electroanal. Chem.* **391** (1995) 199 - 201
- [17] D. Nocera, *Acc. Chem. Res.* **45** (2012) 767 - 776
- [18] B. Gholamkhash, H. Mametsuka, K. Koike, T. Tanabe, M. Furue, O. Ishitani, *Inorg.Chem.* **44** (2005) 2326–2336
- [19] J. Mao, K. Li, T. Peng, *Catal.Sci.Technol.*, **3** (2013) 2481 - 2498

- [20] T. Arai, S. Sato, K. Uemura, T. Morikawa, T. Kajino, T. Motohiro, *Chem. Commun.* **46** (2010) 6944 - 6946
- [21] E. E. Barton, D. M. Rampulla, A. B. Bocarsly, *J. Am. Chem. Soc.* **130** (2008) 6342 – 6344
- [22] E. I. Lan, J. C. Liao, *Metab. Eng.* **13** (2011) 353 - 363
- [23] G. Diekert, *FEMS Microbiol.Lett.* **87** (1990) 391 - 395
- [24] M. Kuroda, T. Watanabe, *Energy Cowers.* **36** (1995) 787-790
- [25] M. Aresta, E. Quaranta, I. Tommasi, *J. Chem. Soc., Chem. Commun.* **7** (1988) 450 - 452
- [26] M. Aresta, E. Quaranta, R. Liberio, C. Dileo, I. Tommasi, *Tetrahedron* **54** (1998) 8841 - 8846
- [27] O. Heichal-Segal, S. Rappoport, S. Braun, *Biotechnol.* **13** (1995) 798 - 800
- [28] D. W. Kim, J. H. Yang, Y. K. Jeong, *Appl. Microbiol.Biotechnol.* **28** (1988) 148 - 154
- [29] A. Lindgren, O. Gorton, T. Ruzgas, U. Baminger, D. Haltrich, M. Schülein, *J. Electroanal. Chem.* **496** (2001) 76 - 81
- [30] U. Ruschig, U. Müller, P. Willnow, T. Höpner, *Eur. J. Biochem.* **70** (1976) 325 - 330
- [31] Y. Lu, Z. Jiang, S. Xu, H. Wu, *Catal. Today* **115** (2006) 263 - 268
- [32] R. Obert, B. C. Dave, *J. Am. Chem. Soc.* **121** (1999) 12192 – 12193
- [33] S. Kuwabata, R. Tsuda, H. Yoneyama, *J. Am. Chem. Soc.* **116** (1994) 5437 - 5443
- [34] T. Reda, C. M. Plugge, N. J. Abram, J. Hirst, *PNAS* **105** (2008) 10654 - 10658
- [35] S.Schlager, D. Hiemetsberger, A. Wagner, D. H. Apaydin, E. Portenkirchner, N.S. Sariciftci, *Nature Science* (2013), submitted
- [36] S. Datta, L. R. Christena, Y. R. S. Rajaram, *Biotech.* **3** (2013) 1 - 9
- [37] J. V. B. Kozan, R. P. Silva, S. H. P. Serrano, A. W. O. Lima, L. Angnes, *Anal. Chim. Acta* **591** (2007) 200 - 207
- [38] H. Takahashi, B. Li, T. Sasaki, C. Miyazaki, T. Kajino, S. Inagaki, *Micropor. Mesopor. Mat.* **44 - 45** (2001) 755 - 762
- [39] J. Fu, J. Reinhold, N. W. Woodbury, *PLoS One* **6** (2011) e18692
- [40] H. Hsieh, P. Liu, W. Liao, *Biotechnol. Lett.* **22** (2000) 1459 - 1464

- [41] Q. Shi, Y. Tian, X. Dong, S. Bai, Y. Sun, *J. Biochem. Eng.* **16** (2003) 317 - 322
- [42] M. Sardar, M. N. Gupta, *Enzyme. Microb. Tech.* **37** (2005) 355 - 359
- [43] Q. Shen, R. Yang, X. Hua, F. Ye, W. Zhang, W. Zhao, *Process. Biochem.* **46** (2011) 1565 - 1571
- [44] B. Krajewska, *Enzyme. Microb. Tech.* **35** (2004) 126 - 139
- [45] H. Wen, V. Nallathambi, D. Chakraborty, S. C. Barton, *Microchim. Acta* **175** (2011) 283 - 289
- [46] M. J. Swann, D. Bloor, T. Haruyama, M. Aizawa, *Biosens. Bioelectron.* **12** (1997) 1169 - 1182
- [47] D. L. Nelson, Lehninger, Principles of Biochemistry, 4th Edition, W. H. Freeman ed.
- [48] A. Wurtz, *Comptes Rendus Hebdomadaires des Séances de l'Académie des Sciences, Paris* **91** (1880) 787 - 791
- [49] V. Henri, Lois générales de l'action des diastases, *Hermann, Paris* 1903